Progress in Oceanography 207 (2022) 102866

Contents lists available at ScienceDirect

Progress in Oceanography

journal homepage: www.elsevier.com/locate/pocean

Geophysical controls on metabolic cycling in three Patagonian fjords

Joseph R. Crosswell [a,*], Francisco Bravo [b], Iván Pérez-Santos [c,d,e], Geoffrey Carlin [a], Nagur Cherukuru [f], Cassie Schwanger [g], Rob Gregor [g], Andrew D.L. Steven [a]

[a] CSIRO Oceans and Atmosphere, 41 Boggo Rd., Dutton Park, QLD 4102, Australia
[b] CSIRO Chile, Av. Apoquindo 4700, Floor 9, Las Condes, Santiago, Chile
[c] Centro i-mar de la Universidad de los Lagos, Puerto Montt, Chile
[d] Center for Oceanographic Research COPAS Sur-Austral and COPAS COASTAL, Universidad, de Concepción, Chile
[e] Centro de Investigaciones en Ecosistemas de la Patagonia (CIEP), Coyhaique, Chile
[f] CSIRO Oceans and Atmosphere, Clunies Ross St., Black Mountain, ACT 2601, Australia
[g] CSIRO Oceans and Atmosphere, Castray Esplanade, Battery Point, TAS 7004, Australia

ARTICLE INFO

Keywords:
Coastal
Carbon
Nutrients
Biogeochemistry
Hydrodynamics
Morphology
Chile
Patagonia
Chiloe sea

ABSTRACT

Biogeochemical cycling in fjords underpins crucial environmental and economic functions including carbon sequestration and food security, and a fundamental understanding of the controls on these cycles is essential for sustainable management of fjords that are facing increasing climate and anthropogenic stressors. However, the interaction of external forcing and local geomorphology in fjords leads to complex coupling that is challenging to measure using traditional methods, particularly in a connected coastal system like the Chiloe Inland Sea (CIS) in northern Patagonia. This study resolves key functional differences between the three major fjords (Reloncaví, Comau and Reñihue) in the CIS using high-resolution sampling of surface waters integrated with regional oceanographic and meteorological observations, models and historic data. The dominant geophysical control varied among the three fjords: river input in Reloncaví Fjord, synoptic winds in Comau Fjord and tidal forcing in Reñihue Fjord. Variable geomorphic characteristics, e.g., orientation and the location of the riverine input, resulted in contrasting physical-metabolic responses between fjords to otherwise similar meteorological and oceanic forcing conditions. Each fjord's relative location and degree of connectivity to the CIS influenced its internal metabolic balance over synoptic to seasonal scales. In Comau Fjord, the salt fingering form of double diffusive mixing was linked to vertical density structure and wind forcing in the northern CIS; consistent trends in historical data suggest that salt fingering may be an important mechanism for delivery of nutrients to the euphotic zone. The highest metabolic rates in the study region occurred in Reñihue Fjord and were linked to vertical mixing of nutrient-rich waters to the surface in the central CIS. Climate change is predicted to result in decreasing river discharge and weakening zonal winds in northern Patagonia. Therefore, the functional relationships observed in this study imply-two key impacts of these altered forcing conditions in coming decades: 1) a lateral shift in the transfer of planktonic carbon to coastal sediments, i.e., moving landward from the CIS into fjords, and 2) greater biogeochemical variability in fjord surface waters, which will present greater management challenges for aquaculture.

1. Introduction

Fjords are highly dynamic environments, and many temperate fjords are productive coastal systems that support important fisheries, aquaculture and biodiversity (Iriarte et al., 2010; Torres et al., 2011; Bianchi et al., 2020). Fjords have also been recently identified as globally significant carbon sinks; organic carbon (OC) burial in fjords is estimated to be the highest per unit area in the world, accounting for 11% of marine carbon burial (Smith et al., 2015). These key ecosystem functions combined with their linkage to land, ocean, cryosphere and atmosphere has led to the designation of fjords as Aquatic Critical Zones that are highly sensitive to climatic and anthropogenic stressors and warrant intensive investigation (Bianchi et al., 2020). While fjords are generally classified as deep, strongly stratified estuaries, individual fjords display unique hydrodynamic behavior that is determined by the interaction of regional-scale ocean–atmosphere dynamics with local geomorphologic

* Corresponding author.
E-mail address: Joey.Crosswell@CSIRO.au (J.R. Crosswell).

https://doi.org/10.1016/j.pocean.2022.102866

Available online 10 August 2022

features (Farmer and Freeland, 1983; Cottier et al., 2010; Inall and Gillibrand, 2010; Geyer and Ralston, 2011). These physical processes in turn control biogeochemical functioning that sustain ecosystem services like carbon sequestration and carrying capacity for aquaculture (Iriarte et al., 2010; Stigebrandt, 2012; Almonacid and Medel, 2020). Accordingly, characterizing the coupling of geophysical drivers and metabolic cycles across multiple scales is critical to understand the role and response of fjords to projected change in climate and anthropogenic development.

While much of the research on fjords over the past century focused on northern hemisphere systems, study of Patagonian fjords has expanded substantially over recent decades in tandem with the burgeoning Chilean aquaculture industry, which in 2018 was the world's second largest producer for salmonid and bivalve aquaculture (FAO, 2020). Large-scale oceanic and atmospheric forcing of Patagonian fjords has been examined across a range of timescales, from multi-annual variability associated with the El Niño–Southern Oscillation to synoptic-scale variability of atmospheric pressure systems (Narváez et al., 2019; Pérez-Santos et al., 2019; Saldías et al., 2021). These climate-ocean drivers have been linked to trends in observational time series, such as decreasing river discharge since the 1970s (León-Muñoz et al., 2013) and seasonal shifts in water mass exchange and phytoplankton community composition (Pérez-Santos et al., 2021). Hydrodynamic studies have identified system-specific processes among Patagonian fjords including wind-driven seiches (Castillo et al., 2017), 2- and 3-layer circulation (Valle-Levinson et al., 2014), double-diffusive mixing (Pérez-Santos et al., 2014) and seasonal renewal driven by external density fluctuation and wind stress (Aiken, 2012; Pinilla et al., 2020). These hydrodynamic processes exert direct control on carbon flows to and within fjords (Vargas et al., 2018; González et al., 2019; Vergara-Jara et al., 2019). Carbon cycling in fjords can also be influenced by local lithological and glacial characteristics such as glacier presence and type, fjord-glacier geometry and lithogenic matter in freshwater inputs, which can generate variable responses to changing conditions ranging from ballasting to destabilizing carbon flows (Smith et al., 2015; Hopwood et al., 2020; Seifert et al., 2019; Bianchi et al., 2020; Marshall et al., 2021). In Patagonia, these glacial fjords predominantly occur at latitudes above ~46°, whereas at lower latitudes, i.e. north Patagonia, glaciers are restricted to high elevations and fjords are directly connected to river networks. Controls on river-borne allochthonous carbon primarily influence air–water fluxes and sediment deposition in riverine-dominated regions (Sepúlveda et al., 2011; Silva et al., 2011; Mayr et al., 2014), whereas controls on the production and transformation of autochthonous OC involve more complex and variable pathways such as rapid metabolic cycling in surface waters. Although euphotic surface waters generally comprise a small portion (<30 m depth) of the water column in deep fjords, biogeochemical processes in this shallow surface layer play an outsized role in the long-term fate and global implications for OC storage in fjords. Metabolic balance in these surface waters is constrained by hydrodynamic-biogeochemical coupling that regulates a biological carbon pump whereby autochthonous OC generated in surface waters is exported to long-term storage in deep sediments or is consumed by grazers to form the base of marine food webs.

Patagonian rivers generally have low nitrogen and phosphorus concentrations and thus form a nutrient-deplete surface layer where they discharge into fjords. This buoyant lens of estuary water acts as a control on primary production by separating the primary resources required for photosynthesis, i.e., light at the surface and nutrients in subpycnal waters (Iriarte et al., 2010; Calvete and Sobarzo, 2011). The interactions of physical processes noted above with fjord geomorphology modulate this light-nutrient partitioning and thereby influence primary productivity, e.g., by facilitating freshwater export/retention, upwelling and vertical mixing (González et al., 2010, González et al., 2011, González et al., 2013; Montero et al., 2017). Metabolic balance is also influenced by the amount and quality of organic matter, silicic acid and nutrients in riverine water, as well as point source inputs, particularly from aquaculture (Mulsow et al., 2006; Iriarte et al., 2013; Mayr et al., 2014; Olsen et al., 2014; Olsen et al., 2017).

Despite extensive investigations, there remain several gaps in the functional understanding of physical-metabolic coupling in Patagonian fjords (Iriarte, 2018). First, nearly all metabolic measurements have used incubation methods that inherently separate biological activity from dynamic physical processes (Regaudie-de-Gioux et al., 2014; Dokulil and Qian, 2021). Recent advances in observational tools present two possible solutions for free-water metabolic measurements: 1) fast repetition rate fluorometry, a proxy-based method that can resolve instantaneous photosynthetic dynamics, but still requires further development of conversion factors (Hughes et al., 2018); and 2) high-resolution measurement of the carbonate system to quantify respiration and primary productivity over diel and longer cycles (Crosswell et al., 2017; Crosswell et al., 2020). To date, neither method has been extensively applied in fjords. The second challenge is the need for integrative research activities that constrain relevant scales of time and space in highly connected fjord systems, e.g., comparing regions with multiple fjords under similar forcing conditions from diel to interannual cycles. While there has been recent progress in representing broad-scale processes along the Patagonian coast using regional coastal models, resolution of finer-scale forcing within fjords remains poor (Skogseth et al., 2007; Steven et al., 2019; Almonacid and Medel, 2020; Ruiz et al., 2021). Moreover, there is a paucity of observational studies that constrain relevant processes across multiple scales, which are essential to construct and validate models.

This study employed an integrative approach to examine geophysical-metabolic coupling in the three northernmost fjords in Patagonia. The overarching goal of this work was to characterize dominant drivers and biogeochemical processes, particularly leveraging insight from comparing multiple systems under similar seasonal conditions. Direct observations primarily focused on surface waters via high-resolution measurements over tidal and diel scales during a research cruise in the austral fall of March 2018 (Crosswell, 2018). These observations were combined with meteorological and historical data as well as model outputs to assess the relative contributions of winds, tides, rivers and local geomorphology within and between fjords. To synthesize data from multiple study systems and sources, we first describe environmental forcing and direct biogeochemical observations before quantifying dynamic processes; additional model simulation and historical data are visualized in supplementary files. We then examine the dominant forcing mechanisms and their control on metabolic function in each fjord. Finally, we interpret the implications of projected climate change for carbon storage and aquaculture in these fjords over coming decades.

2. Methods

2.1. Study site

The northern Patagonian fjord system is formed by complex and irregular topographic features dominated mainly by fjords (e.g., Reloncaví, Comau, Reñihue, Piti Palena, Puyuhuapi, Aysén, Quitralco and Cupquelan). All fjords are located in the eastern side of the Patagonian region, being in direct contact with the continent and therefore receiving freshwater input from rivers and ice melting (Dávila et al., 2002; Calvete and Sobarzo, 2011). The annual cycle of river discharge reaches a minimum in austral summer and maximum in winter, with a second and smaller peak occurring in spring due to snowmelt (León-Muñoz et al., 2013). Fjords are connected to the Chilean Inland Sea (CIS) which contains large open-water areas such as the Ancud and Corcovado Gulfs (Fig. 1). Channels mediate water exchange between the CIS and the Pacific Ocean and also between gulfs and fjords, e.g., Chacao, Apio, Guafo, Moraleda, Jacaf (Pérez-Santos et al., 2014; Pinilla et al., 2020;

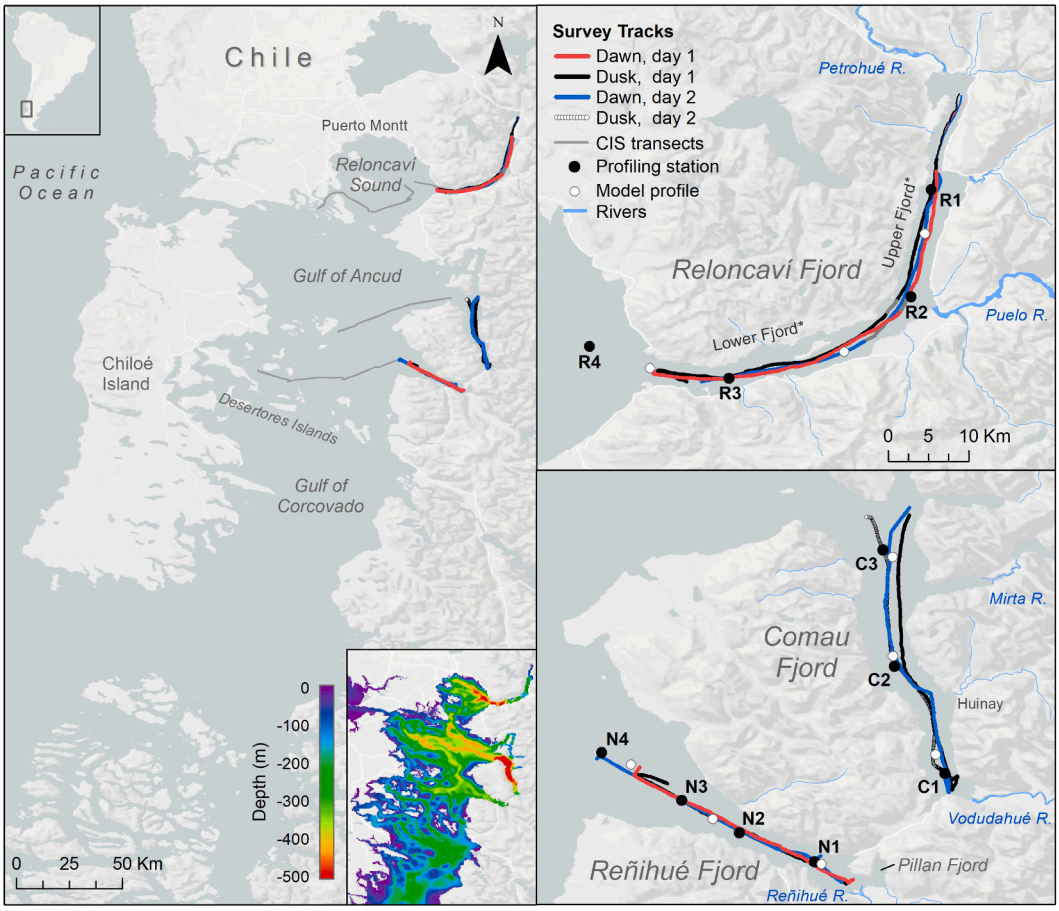

Fig. 1. Map of Chiloe Sea showing dawn-dusk survey tracks in the three study systems. *Reloncaví Fjord was divided into upper and lower regions based on the region of minimum salinity (grey) during each survey. Data from the northern ~10 km "head region" (narrow lines) of Reloncaví Fjord were excluded from metabolic analyses, as salinities in this region were not comparable between dawn-dusk surveys (Fig. 4).

Ruiz et al., 2021). Water masses in Patagonian fjords are generally classified based on salinity (Sievers, 2008; Sievers and Silva, 2008). Estuarine water (EW) occupies the top ~10 m of the water column with a salinity range of 0–31. Below this layer, Modified Subantarctic water (MSAAW) is represented by salinities between 31 and 33. This water mass forms by mixing of EW with Subantarctic water (SAAW) and is typically observed to ~100 m (Pérez-Santos et al., 2014; Schneider et al., 2014; Quiroga et al., 2016). However, in Reloncaví Sound and Reloncaví Fjord, MSAAW has been shown to extend to the seabed (250–400 m) (Castillo et al., 2016; Pérez-Santos et al., 2021). SAAW occurs below the MSAAW and has a salinity range of 33–33.8. SAAW is formed north of the polar front and influences all the exterior coast of the Patagonian fjords system, entering the interior fjords by the channels and gulfs connected to the Pacific Ocean (Crawford et al., 2021). Finally, Equatorial Subantarctic water (ESSW) with salinities over 33.8 occurs as a deep layer close to the seabed (e.g., in Puyuhuapi Fjord and Jacaf Channel). However, the topography of the southern Corcovado Gulf acts as a physical barrier limiting the deep transport of ESSW into the CIS (Silva, 2008; Schneider et al., 2014).

Recently, Pérez-Santos et al. (2021) characterized seasonal nutrient trends in Reloncaví Sound over a three-year monthly time series, which represents the best-resolved biogeochemical time series in the northern Patagonian fjord system to date. This time series showed that inorganic nutrients in the surface layer were maximal during fall-winter, e.g., 2.4 and 24 μM of PO_4 and NO_3, respectively. These nutrients were rapidly consumed by primary production in spring and they (particularly NO_3) remained depleted in the surface layer (0–20 m) through late summer. The annual cycle then repeated as inorganic nutrients increased in fall and winter, mainly due to diminishing primary production and intense vertical mixing by winds and thermal convection. Remote sensing and modelling studies suggest that northeastern waters of the CIS follow similar seasonal trends as those described by Pérez-Santos et al. (2021) (Ruiz et al. 2021; Saldías et al. 2021; Vásquez et al. 2021). However, these regional-scale studies are too coarse to resolve the fjords in this region, where the influence of aquaculture, coastal development and climate change are most concentrated. Accordingly, the three major fjords in the northeastern CIS are the focus of this study. While the absence of a well-defined sill was a common feature among these fjords, they otherwise had divergent physical characteristics.

Reloncaví Fjord is the northernmost fjord in Patagonia and is the longest (55 km) and narrowest (1–3 km) fjord in the CIS, connecting directly to open waters of Reloncaví Sound (Fig. 1). It has variable topographic features, including a 120° bend at the fjord center and several step changes in depth (e.g., ~450, 250, 200 and 50 m; Castillo et al., 2017). At ~10 km from the fjord head, the morphology transitions to a narrow and shallow channel that terminates at the Petrohue River. While this river drains the large and deep Todos Los Santos Lake, the majority of freshwater input to Reloncaví Fjord comes from the Puelo River, which drains a large catchment through a series of mountainous lakes. The Puelo River discharges at the bend in Reloncaví Fjord and accounts for > 80% of freshwater input to the northern CIS from its five largest rivers (Fig. 2). Reloncaví Fjord is among the most well-studied Patagonian fjords due to its proximity to Puerto Montt (Fig. 1), which is the location of the nearest available meteorological and tidal data during the study period (Fig. 3).

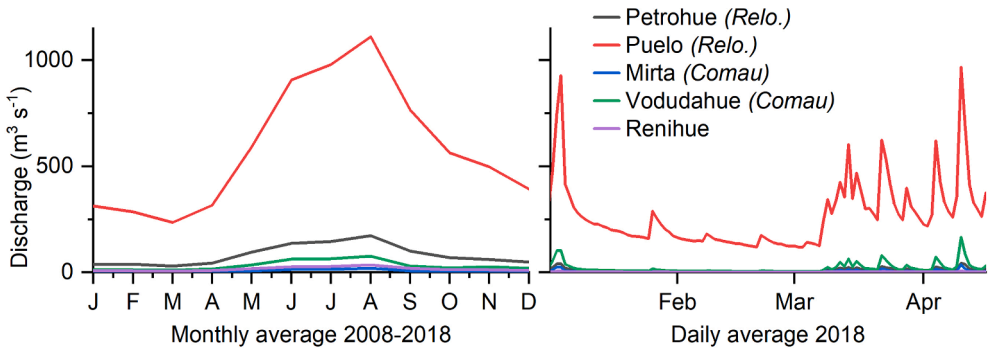

Fig. 2. Modeled river discharge for major rivers in the three study fjords (Steven et al., 2019).

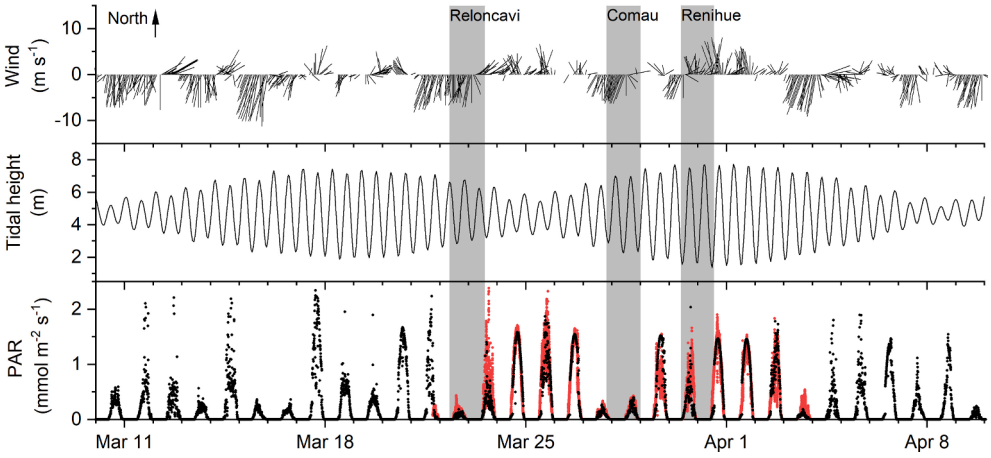

Fig. 3. Wind and tidal height at Puerto Montt and PAR from the research vessel during the voyage (red) and from Huinay Research Station in Comau Fjord (black). Shaded areas show dawn-dusk survey intervals in fjords.

Comau Fjord is the deepest among the three study systems (500 m). It has the form of a narrow funnel (2.5–6.5 km) that opens to the north, where the main channel curves westward connecting to the Ancud Gulf (Fig. 1). Comau Fjord is connected to several subfjords to the east and north, but freshwater input is dominated by the Vodudahue River, which discharges at the fjord head. Unlike the major rivers in the other two study systems, the Vodudahue River directly drains a high relief catchment without substantial buffering from any upstream lakes. A research station at Huinay (Fig. 1; https://www.huinay.cl/) has provided a base for most prior studies in Comau Fjord, including historic meteorological and oceanographic data examined in this study.

Reñihue Fjord has the form of a broad funnel (2.5–12 km, max depth = 280 m) that opens to northwest into waters of the central CIS, which are bounded by the complex morphology of the Desertores Islands (Fig. 1). Reñihue River is the main freshwater source to the fjord but this riverine input is considerably lower than in Reloncaví and Comau Fjords (Fig. 2). The river drains a series of upstream lakes along with steep topography in the lower catchment and terminates at the fjord head via meandering deltaic channels. The fjord head is connected to a small and shallow (<50 m) subfjord, Pillan Fjord, through a tidal channel at the northern margin of the delta (Fig. 1). Reñihue Fjord is the most remote and least studied of the major fjords in the CIS.

2.2. Dawn-dusk surveys and water-column profiles

Spatial surveys in fjords were conducted in March 2018 as part of a 14-day research cruise in the CIS, collecting underway observations along a 1900 km survey track and discrete water column profiles at 42 profiling stations (Crosswell, 2018). For each fjord, a series of three high-resolution spatial surveys were conducted at dawn, dusk and the following dawn or a similar dusk-dawn-dusk sequence (sensu Crosswell et al., 2017). These surveys constrained diel cycles and enabled calculation of physical and metabolic fluxes. Surveys began approximately 1.5 h prior to sunrise or sunset and required about 3 h to cover the entire fjord at a speed of 6–10 knots (Fig. 1). Water was continuously pumped from an intake located ~0.5 m below the water surface to an array of instruments for underway analysis of carbon, nutrients and physico-chemical parameters (Table 1). The instrument array consisted of a series of flow-through cells for continuous measurements with parallel wet chemistry analyzers supplied by filtered sampling lines, as described by Crosswell et al. (2020). The response time for each measurement was determined empirically on each survey for underway data or at each station for water column profiles, and data were lag adjusted to minimize hysteresis. Wind speed, wind direction and photosynthetically active radiation (PAR) were measured at 20 s intervals using an AirMar 150WX weather station and Wetlabs ECO-PAR sensor mounted on a meteorological instrument mast.

Water-column profiles of salinity and temperature were collected while underway using small CTDs on a weighted fishing line that was attached to an electric reel (Table 1). The drag and power sequence were tuned such that when the clutch disengaged, the CTD entered freefall to a depth of about 30 m at which point the clutch reengaged. The CTD then more gradually ascended to the surface and was reeled in before repeating the process. Underway CTD profiling was conducted on all along-axis surveys as well as on several across-axis transects in each fjord between the dawn-dusk surveys.

Water-column profiles were also collected at 3–4 stations in each fjord before, between or after dawn-dusk surveys (Fig. 1). These profiles generally consisted of a first cast to 30 m and then a second cast to 100 m

Table 1
Sampling equipment and methods.

Sampling component	Instrument	Parameters	Resolution	calibration method and interval
Underway surface	YSI EXO2 Sonde	**CTD**: Conductivity, Temperature, Depth	20 s	Cross-calibrated to SBE19, each station
		DO: Dissolved oxygen		Atmospheric calibration, each station
		Chl: Chlorophyll *a* fluorescence		Cross-calibrated to discrete, each station
	Satlantic SUNA V2	**NOx**: Nitrate + Nitrite	120 s	Cross-calibrated to FIA[a], each fjord
	Contros HydroC CO_2	**pCO_2**: Partial pressure of carbon dioxide	20 s	Factory (0–3000 ppm), prior to voyage
	Apollo SciTech AC-S	**DIC**: Dissolved Inorganic Carbon	~180 s	Certified reference material[b], ~12 h
	Metrohm 904 Titrando	**TA, pH**: Total Alkalinity	~380 s	Certified reference material[b], ~12 h
	Global FIA flowtracker	**NO_x**: Nitrate + Nitrite **PO_4**: Phosphate	~460 s, ~340 s	Certified reference material for nutrients in seawater (RMNS), ~12 h
Underway profiling	Van Essen CTD-divers (6)	**CTD**	1 s (0.3 m)	Cross-calibrated to SBE19, each station
Station profiling	YSI EXO2 Sonde	same as underway	1 s (0.1 m)	same as underway system
	Seabird SBE19plusV2	**CTD**	1 s (0.1 m)	Factory, immediately prior to voyage
	Satlantic SUNA V2	**NOx**	1 s (0.1 m)	Cross-calibrated to FIA[a], each station
	Satlantic HyperPro II	**PAR**: photosynthetically active radiation	0.5 *m*	Factory, prior to voyage
	Discrete (Niskin)[c]	Photopigments via HPLC	surface	(Clementson et al., 2020)
	Discrete (Niskin)[d]	**DIC, TA, pH, NO_x, PO_4**	~100 *m*	Same as underway system
Met[e]	AirMAR 150WX	Wind speed and direction	20 s	Factory
	Wetlabs ECO PAR	**PAR**	20 s	Factory

[a] Underway SUNA data were binned by fjord and calibrated using multiple linear regression for salinity, temperature and time (i.e. drift); CDOM was not statistically significant in the regression. SUNA profiles were calibrated using a simple linear regression with discrete samples at each respective station.
[b] Obtained from AG Dickson at Scripps Institute of Oceanography.
[c] Discrete samples for photopigments were immediately flash frozen and returned to Australia for analysis.
[d] Discrete samples from depth were immediately run on the wet chemistry instruments in the underway system.
[e] Meteorological: Mounted on mast 9 m from water surface.

for measurement of inherent optical properties and biogeochemical parameters, respectively (Table 1). Discrete samples listed in Table 1 were collected at the surface, 100 m and 200–250 m using a Niskin bottle. Samples from additional depths were collected in waters shallower than 200 m, depending on the total depth. Discrete samples for phytoplankton pigments (Clementson et al., 2020) were collected from the surface only.

2.3. Metabolism

The fjords were assumed to be in a steady state over the dawn-dusk sampling period in terms of salt balance. Accordingly, salinity was used as a conservative tracer to constrain metabolic rates for a given water mass, denoted herein as fluxes. Data were grouped within salinity intervals, defined herein as bins. A salinity interval between 1.5 and 2.0 per bin was chosen for each fjord, depending on which bin size showed the most even distribution of total observations per bin. This approach allowed approximately the same water mass to be tracked despite spatial displacement between surveys due to wind and tidal forcing. Distance-weighted averages for all parameters were determined for each bin on each survey to remove any potential bias from variable survey speed, e.g., due to winds and currents. The salinity bounds for metabolic estimates were inherently limited to salinities that were observed on all three surveys. Thus, these bounds excluded regions of episodic upwelling or riverine input where steady-state assumptions were likely to be invalid over the short timescales of this study.

Gross Primary Production (GPP), ecosystem respiration (R), and net ecosystem production (NEP) were determined based on the change in DIC concentration between surveys. For each salinity bin, the hourly metabolic DIC flux (F) was calculated based on the difference between the dawn1-dusk (F_1) surveys and the dusk-dawn2 (F_2) surveys (Eqs. (1)–(2)):

$$F = (\Delta DIC_n - \frac{f_g}{z_s}) \quad (1)$$

$$\Delta DIC_n = (m(\bar{s} - s_2) + DIC_2) - (m(\bar{s} - s_1) + DIC_1) \quad (2)$$

where ΔDIC_n is the change in the salinity-normalized DIC concentration between subsequent surveys and f_g is the portion of ΔDIC_n that is due to air–water CO_2 exchange (details of f_g calculations in Section 2.4). The surface layer depth (z_s) was determined by binning densities (ρ) for each underway CTD profile to 0.5 m depth intervals, averaging these data into a single survey-specific profile for each surface salinity bin, then finding the maxima of $d\rho/dz$. If multiple layers were apparent, then z_s was the shallowest local maxima. In Eq. (2), m is the fjord-specific slope of the DIC:salinity relationship determined using the distance-weighted averages for each bin on each survey; $\bar{s}$ is the bin-specific salinity average for all three surveys, while s and DIC are respectively the bin-specific salinity and DIC averages on individual surveys. Daily R, GPP and NEP for each bin were determined following Eqs. (3)–(6):

$$F_d = \frac{F_1 \cdot t - F_2 \cdot t_{ex}}{t + t_{ex}} \quad (3)$$

$$F_n = \frac{F_2 \cdot t - F_1 \cdot t_{ex}}{t + t_{ex}} \quad (4)$$

$$R = F_n \cdot 24 \quad (5)$$

$$GPP = Dl \times F_d + F_n(24 - Dl) - R \quad (6)$$

$$NEP = GPP - R \quad (7)$$

where F_d and F_n are the hourly DIC fluxes for day and night respectively, t is hours between the subsequent surveys for the relevant interval and t_{ex} is hours of t that exceeded the relevant day-night light period. Eq. (3) was required to adjust for cases where bins were sampled before dawn or after dusk due to 3 h survey times. The day length (Dl) was quantified as the number of hours when the surface irradiance at the vessel-mounted PAR sensor was above a threshold of five μmol photons m^{-2} s^{-1}. This threshold was selected as a clear demarcation between night and day, as the photon flux changed rapidly around this value and

it avoided potential noise at lower thresholds.

Although directly-measured DIC would be the most suitable parameter for metabolic calculations, a faulty mass flow controller led to unknown quality of some underway DIC data, except when closely monitored. Instead, DIC data applied in Eqs. (1)–(2) was calculated from TA and pCO_2 using CO2SYS (Version 2.3, https://cdiac.ornl.gov/ftp/co2sys/), with dissociation constants from Millero (2010), the total pH scale, and the in situ salinity and temperature. First, a conservative TA:salinity relationship was confirmed across the relevant salinity range in each fjord (Fig. S1). The fjord-specific TA:salinity regression was then used to interpolate TA data at 20 s resolution. A three-minute moving average was applied to TA, salinity and temperature in order to normalize instrument response times with pCO_2 data. Finally, DIC was calculated in CO2SYS and validated against directly-measured DIC that were of verifiable quality, i.e., incremental periods throughout each survey interval when DIC analysis was closely monitored.

Uncertainty in metabolic terms was calculated following Lehrter and Cebrian (2010) and represented as the 95 % confidence interval. Briefly, the standard error was calculated for each salinity bin based on the standard deviation and number of salinity observations combined with the uncertainty in the TA:salinity regression for the respective salinity range. Uncertainty was then propagated through Eqs. (1)–(7) ignoring analytical uncertainty, which was determined to be insignificant based on instrument calibration data. Uncertainty in free-water metabolic measurements can arise when deviation from steady-state conditions occurs due to variable point source inputs over diel timescales. Volcanic vents have been identified as one such point source in Comau Fjord (e.g., Fillinger and Richter, 2013) and may occur in other fjords and regions of the CIS due to the prevalence of volcanic activity. While these vents emit DIC and nutrients, Muñoz et al. (2014) reported that input of vent fluids in Comau are low and do not substantially influence bulk water chemistry. Furthermore, we found no evidence of elevated DIC or nutrients that would indicate a notable vent fluid signal during 2017 and 2018 surveys (Crosswell, 2017; Crosswell, 2018). Regardless, deviations from steady state due to point source input or other sources, such as direct precipitation to surface waters, are inherently included in the uncertainty calculation described above.

2.4. Air-water fluxes

Air-water CO_2 fluxes were calculated between each survey interval using distance-weighted averages of pCO_2, temperature and salinity within each bin following Eqs. (8)–(9).

$$f_g = K_0(k_{660})(\Delta pCO_2)(Sc/660)^{-0.5} \tag{8}$$

where K_0 and Sc are the solubility coefficient and Schmidt number at ambient surface temperature and salinity (Weiss, 1974; Wanninkhof, 2014) and ΔpCO_2 is the air–water pCO_2 gradient. Atmospheric pCO_2 was assumed to be constant at 400 µatm. Positive ΔpCO_2 and air–water fluxes indicate CO_2 efflux from the water to the air. The gas exchange coefficient (k_{660}) was determined based on the windspeed (u_{10}) parameterization by Banko-Kubis et al. (2019) for fjords (Eq. (9)).

$$k_{660} = 0.138u_{10}^2 + 3.60 \tag{9}$$

where u_{10} was quantified between respective survey intervals as the temporal average of the true windspeed from the vessel-mounted anemometer.

2.5. Primary productivity model

GPP-Irradiance relationships were determined by combining the planktonic photosynthesis-light curve (PE curve) from Jassby and Platt (1976) and the time-integrated model from Behrenfeld and Falkowski (1997) to yield Eq. (10).

$$\sum GPP = \int_{z_1}^{z_2} P^b_{max}\tanh(\alpha E(z)/P^b_{max})\cdot Dl\cdot Chl(z)dz \tag{10}$$

where P^b_{max} is the maximum light-saturation rate of photosynthesis constrained by Calvin cycle reactions with units of mg-C (mg-chl-a)$^{-1}$h^{-1};α is the photosynthetic efficiency term, which controls the initial slope of the PE curve, and $E(z)$ is the irradiance at depth z. *Chl* in the surface mixed layer was assumed to be uniform such that $Chl(z)$ was equal to the average flow-through chl-a measurement in the respective salinity bin. The irradiance-depth dependence was represented as Eq. (11).

$$E(z) = E_0 e^{-Kd(s)\cdot z} \tag{11}$$

where E_0 is the surface irradiance and $Kd(s)$ is the diffuse attenuation coefficient for downwelling irradiance as a function of salinity. The *Kd*: salinity dependence was determined empirically in each fjord by fitting Eq. (11) to corresponding water column profiles of salinity and irradiance at discrete profiling stations.

The PE curve was expected to vary within the study region depending on nutrient limitation (e.g., Behrenfeld et al., 2002) as well as rates of photoacclimation and physical transport. Thus, an inversion approach using integrated values for GPP and irradiance in respective salinity bins was used to first identify and categorize PE curves under these variable conditions. That is, the GPP term that was calculated as described in Section 2.3 represents the time- and depth-integrated value in surface waters between dawn and dusk surveys. This GPP term was then plotted relative to a similarly integrated irradiance term, thereby allowing data to be grouped based on apparent logarithmic relationships. Finally, PE curves were constructed for each group by solving for P^b_{max} and α in Eq. (10) using the Levenberg–Marquardt algorithm.

The primary productivity model (Eqs. (10)–(11)) was used with water column profiles and time series data to assess vertically-integrated GPP (henceforth PP_I) under monthly-averaged light conditions. K_d and chl-a were directly observed at each discrete profiling station. E_0 was the daily average PAR observed at the Huinay Research Station from 9 March to 8 April 2018. The most appropriate α and P^b_{max} terms were applied to respective water column layers depending on the conditions. For example, the α and P^b_{max} terms that were determined in nutrient-rich surface waters on dawn-dusk surveys were applied to other similarly nutrient-rich layers of the water column.

2.6. Hydrodynamics

Thermodynamic controls on vertical mixing of the water column were examined by calculating the Turner angle (*Tu*) along the depth profile for individual CTD casts. The *Tu* term is an angular expression of convective mixing regimes that depends on the combined influence of salt and temperature gradients. *Tu* profiles were calculated using observational data from underway CTD profiles as well as at discrete vertical profiling stations. First, the measured salinity and temperature data were converted to the standardized terms of absolute salinity (S_A) and conservative temperature (Θ) following the International Thermodynamic Equation of Seawater 2010 (IOC et al., 2010) and using the Gibbs Seawater Oceanographic Toolbox for Matlab (version 3.06.3, McDougall and Barker, 2011). S_A and Θ profiles were then used to calculate *Tu* using the gsw_Turner_Rsubrho function of the Gibbs Seawater toolbox and by iterating through each cast.

Controls on horizontal transport within the fjords were examined based on output from a three-dimensional finite-difference hydrodynamic model of the Los Lagos Region (Herzfeld, 2006; Herzfeld, 2018). This 'Los Lagos Model' was developed as part of an initiative for managing the Chilean aquaculture industry, and observations from this study contributed to model validation (Steven et al., 2019). Here, we extracted modeled current velocities from three grid-cell columns in each fjord (Fig. 1) for March 2018. Cell depths for each hourly interval

were determined based on tidal height, and along-axis velocity components were calculated for each cell column based on the local orientation of the fjord. Additionally, the magnitude of the velocity vector was represented as "absolute velocity" to examine physical forcing independent of direction.

The effect of Earth's rotation on baroclinic exchange in the study systems were quantified using the Rossby radius of deformation (L_R) following Eq. (12) and by assuming two-layer stratification.

$$L_R = \frac{1}{f}\left(\frac{g\rho_2 z_1 z_2}{(\rho_2 - \rho_1)(z_1+z_2)}\right)^{1/2} \quad (12)$$

where f is the Coriolis parameter, g is gravitational acceleration, and z_1, z_2 and ρ_1, ρ_2 are the average depths and densities of the surface and bottom layers, respectively. Within each fjord, L_R was calculated for each salinity bin (Section 2.3), and the corresponding fjord width (w) at the along-axis location of each salinity bin was estimated to define L_R/w ratios. Cross-fjord variation in flow due to rotational effects generally occur when L_R/w > 1 (Cottier et al., 2010).

3. Results

3.1. Environmental forcing conditions

Tides were semidiurnal and displayed little variation within the study region. Comparison of tidal data at Puerto Montt and Huinay (Fig. 3) from 2016 to 2018 showed that differences in tidal phase and amplitude between sites were<0.5 h and 0.3 m, respectively. By contrast, riverine input between fjords differed by three orders of magnitude but were otherwise consistent with seasonal trends (Fig. 2, Section 2.1). From January to March 2018, the Puelo River discharge was 11% lower than the 10-year mean, but still accounted for 90% of the riverine input from the five largest rivers in the study region.

Surface winds at Puerto Montt and in the open waters of the CIS (Figs. 3, S2) reflected synoptic-scale processes that occur on timescales of days to weeks and spatial scales of 100–5000 km (Pérez-Santos et al., 2019). Northerly winds during the study period were associated with low atmospheric pressure systems and resulted in lower PAR due to dense cloud cover (Fig. 3). Southerly winds were associated with high atmospheric pressure systems and resulted in clearer skies and higher PAR. Comparison of PAR data from the vessel-mounted sensor and the Huinay Research Station showed similar trends despite the large area covered during the research voyage (Fig. 3). Consistent PAR across the study region indicated that light availability was primarily controlled by large-scale meteorological forcing rather than orographic cloud formation influenced by local topography.

Surface winds within fjords reflected competing meteorological processes at local scales. Winds were generally channeled along the axis of the fjord, particularly in narrow regions with steep surrounding topography (Figs. 4, S2). High spatial variability on fjord surveys (Fig. 4) and a daily sea breeze observed at fjord meteorological stations (Fig. S2) were linked to katabatic winds. These winds form as dense air at higher elevations flows down to valleys and displaces air that has been warmed during the day by solar radiation. The dominant winds within the fjords shifted from katabatic to synoptic during periods of denser cloud cover and stronger regional forcing, i.e., during low atmospheric pressure systems.

3.2. Stratification and horizontal gradients

Riverine waters mixed rapidly upon entering the fjords to form a surface lens of EW with salinities ranging from ~4–10 (Fig. 4). Pycnoclines separating the surface lens from underlying waters were generally strongest and deepest near the river mouths. Salinity gradients were the dominant driver of vertical and horizontal density stratification in the upper 10–15 m of all three fjords. The location and magnitude of the primary riverine input and apparent influence of wind led to major differences in vertical stratification and along-axis trends within the three fjords.

For over 25 km in lower Reloncaví Fjord, there was only a minor change in surface salinity (~5) and temperature, and vertical stratification was relatively strong and stable between dawn-dusk surveys (Figs. 4, 5). Conversely, upwelling in upper Reloncaví Fjord led to marked differences in density structure between surveys. Upwelling on the dusk survey brought cooler, saline bottom waters to the surface near the head of the fjord and displaced warmer, less saline waters toward the mouth (Figs. 4, 5). This occurrence of upwelling at low tide and during down-fjord winds suggests that the process was linked to contemporaneous wind forcing rather than tidal forcing. Upwelling was also observed on an across-axis transect at the fjord mouth. Here, the pycnocline sloped from 2 to 4.5 m at the southern shoreline and coincided with strong southerly winds (Figs. 4, S3). The role of wind forcing relative to other controls on upwelling and circulation are further considered in following sections. A layer of moderate salinity and temperature underlying the surface layer was observed throughout the fjord, but showed high spatial displacement and variable thickness (2–10 m) between surveys (Figs. 4, 5).

In Comau Fjord, the pycnocline depth and range of surface salinities progressively increased during dawn-dusk surveys. This trend was linked to up-fjord winds that displaced surface waters toward the fjord head (Fig. 4). These winds stacked less-saline waters in the upper 15 km of the fjord and increased surface salinity in the lower 15 km of the fjord. The brackish layer in Comau was 1–2° warmer than in the other fjords, and the thermocline depth was more consistent along the axis of the fjord (Fig. 5). The decoupled response of the thermocline and halocline to wind forcing indicates horizontal exchange with the Gulf of Ancud rather than upwelling. Across-axis transects showed a gradually sloping pycnocline with lower salinities along the eastern shoreline at the mouth and mid-fjord regions (Fig. S3). The 5–10 m increase in pycnocline depths between dawn-dusk surveys was much larger than could be accounted for by the ~1 m variation in the across-axis pycnocline depth. This consistent across-axis vertical structure confirms that the observed variations in pycnocline depth reflected along-axis displacement of surface waters in response to geophysical drivers, as noted above and further examined in later sections.

Salinities in Reñihue Fjord were much greater than the other two fjords, and minimum salinities were confined to a relatively shallow surface layer of 1–2 m (Fig. 4). This surface layer showed high spatial and temporal variability, and several eddies and fronts were visually observed in the narrow upper fjord through to where the fjord begins to widen. Cross-axis and zigzag transects between dawn-dusk surveys revealed slightly lower salinity waters and mixing fronts occurring south of the central axis of the fjord. Below this surface layer, temperatures in Reñihue showed the lowest vertical variability among the three fjords despite receiving the highest irradiance during the survey interval (Figs. 3, 5). This low temperature gradient was also reflected in station profiles (Fig. 6) and indicates strong vertical mixing.

3.3. Nutrients

Each fjord showed a unique nutrient regime where surface concentration and vertical profiles of NO_x were generally consistent within the respective fjords (Figs. 6, 7). The exception was surface nutrients in upper Reloncaví. Here, nutrient concentrations were relatively low and constant at salinities < 7 but then transitioned to conservative salinity: nutrient relationships in more saline waters (Fig. 7). This conservative, single-slope relationship spanned the entire salinity range where saline waters mixed with freshwater input from the Petrohue River. However, this mixing process appeared to be spatially and temporally limited to periods of upwelling near the fjord head. A NO_x:salinity relationship with three distinct slopes was observed in water column profiles within Reloncaví Fjord and showed close agreement with the same relationship

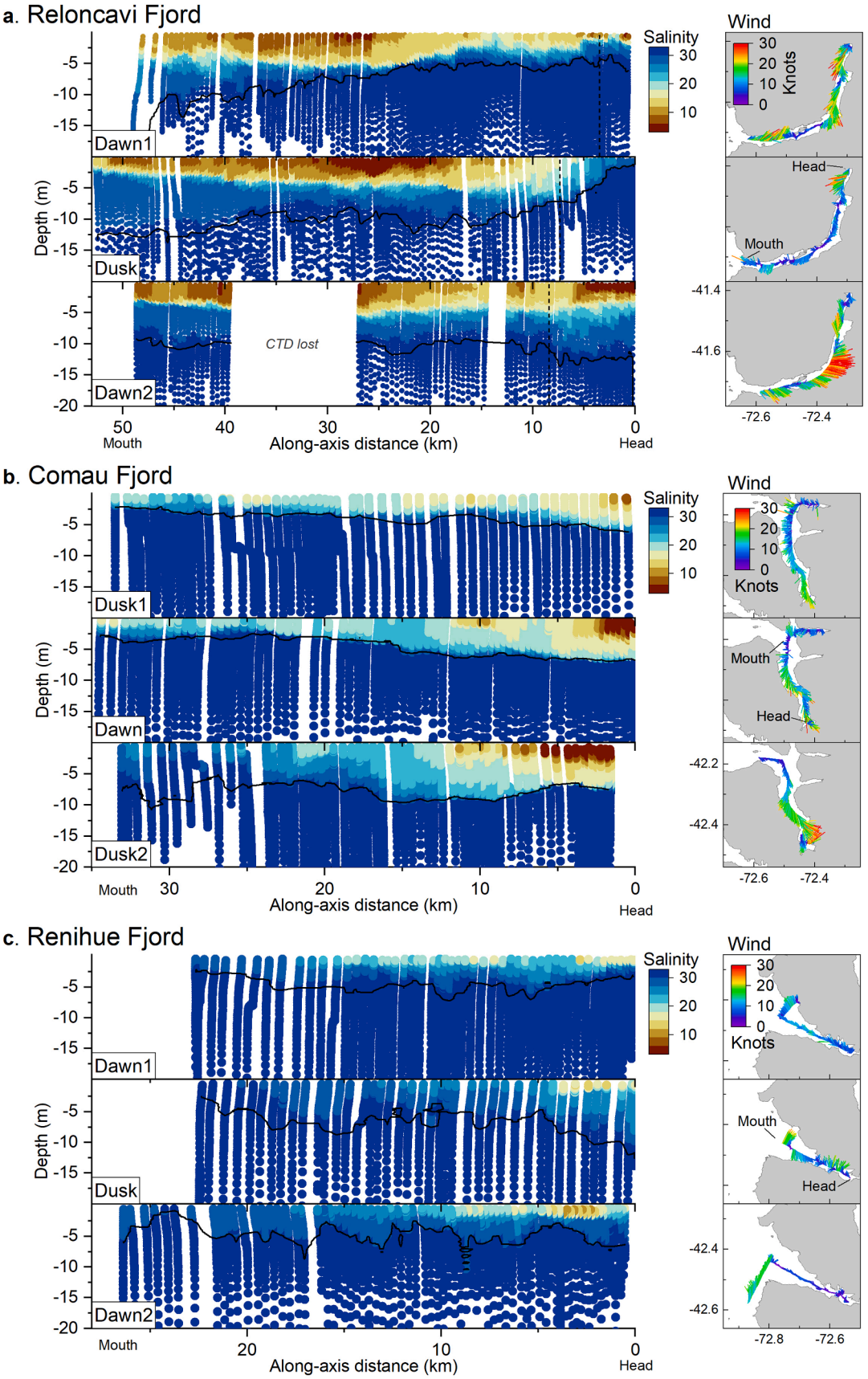

Fig. 4. Depth profiles of salinity (left) and wind vectors (right) during dawn-dusk surveys. Dashed lines show upper boundary of Reloncaví fjord used for metabolism estimates. Black lines show the contour at salinity of 31, representing the barrier between estuary water (EW) and modified subantarctic water (MSAAW) (sensu Sievers and Silva, 2008).

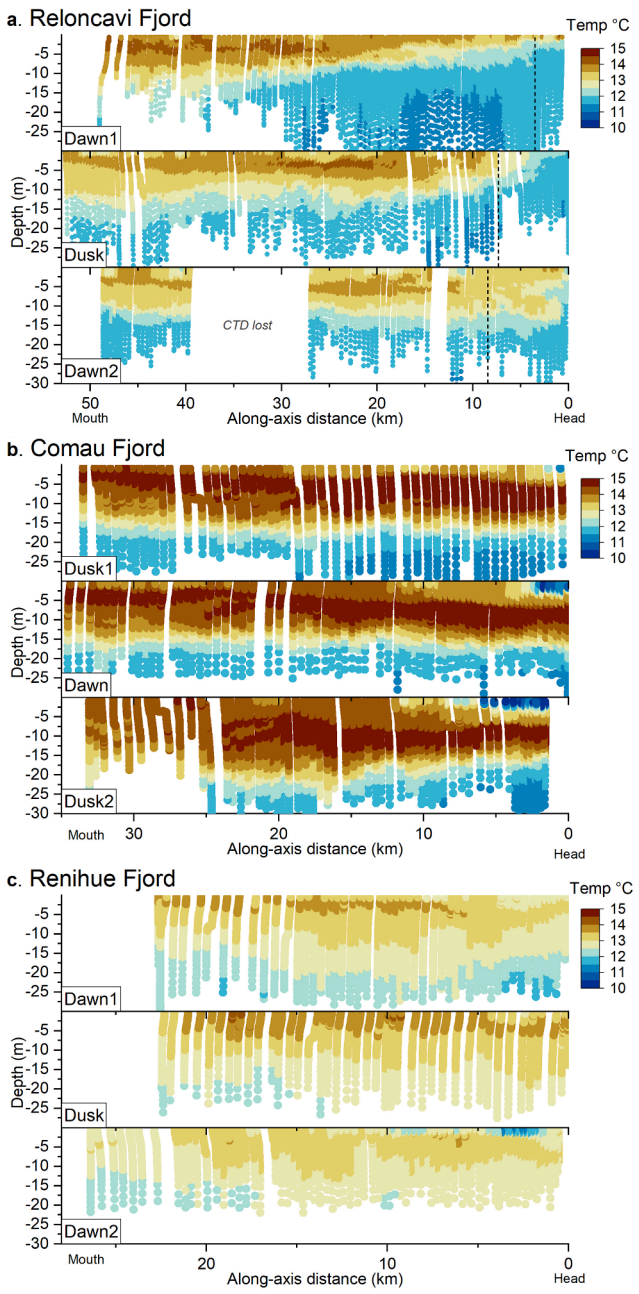

Fig. 5. Depth profiles of temperature during dawn-dusk surveys.

in surface waters of Reloncaví Sound (Fig. 7), suggesting that horizontal transport was the most dominant exchange process during the study period.

In Comau, surface nutrients were below analytical detection limits (NO_x < 0.28 μM, PO_4 < 0.06 μM) throughout the fjord (Fig. 7), and unlike in the other two fjords, the nitricline occurred as a step increase about 10 m below the primary pycnocline (Fig. 6). In Reñihue, surface waters were nutrient rich, and NO_x profiles showed a more linear increase with depth.

Discrete samples from 100 m depth were collected at all profiling stations to compare nutrients at mid-depths between fjords as well as with other regions in the CIS. Nutrients at depth in Comau Fjord (NO_x: 26.4 ± 0.5 μM, PO_4: 2.2 ± 0.1 μM) were the highest among all regions of the CIS, while nutrients in Reloncaví Fjord (NO_x: 23.9 ± 2.9 μM, PO_4: 1.9 ± 0.2 μM) were second highest and comparable to values in Reloncaví Sound (Fig. S4). Nutrient concentrations at depth in Reñihue (NO_x: 20.7 ± 1.8 μM, PO_4: 1.6 ± 0.2 μM) were similar to those in adjoining regions of the CIS.

3.4. Biological indicators and mixing

Dissolved oxygen (DO) and pCO_2 in surface waters followed trends that depended on the end member concentrations of fjord- and region-specific water masses, i.e., rivers and MSAAW, combined with local biological activity. In lower Reloncaví Fjord, conservative trends in DO and pCO_2 relative to salinity reflected estuarine circulation where waters from Reloncaví Sound flow into the fjord as a subpycnal layer and mix with freshwater from the Puelo River (Figs. 6, 7, S5). In upper Reloncaví Fjord, decreasing DO and increasing pCO_2 with salinity reflected mixing of surface waters with waters that were upwelled from greater depths. The maximum DO (104% saturation) and minimum pCO_2 within the fjord were associated with chl-a spikes in the lower Reloncaví (Fig. 7). Reloncaví Fjord showed the lowest DO in shallow subpycnal waters (i.e., < 30 m) among the three fjords (Fig. 6). This subpycnal DO incrementally decreased moving from the fjord mouth toward the fjord head, suggesting consistent landward flow of subpycnal waters combined with progressive DO consumption by net heterotrophy at depth within the fjord. Euphotic depth (1% of surface PAR) ranged from 10 m near the Puelo river mouth to 17.5 m in the upper and lower fjord (Fig. 6). This relatively shallow euphotic depth limited the potential for primary production in subpycnal waters.

Surface waters and subpycnal waters above the nitricline in Comau had the highest DO and lowest pCO_2 among the three fjords. Notably, surface DO saturation remained relatively constant throughout the fjord, varying from ~104 to 108% between dawn-dusk surveys. Maximal chl-a and DO saturation (110–114%) occurred in subpycnal waters at depths of < 10 m and were comparable to values in surface waters outside of the fjord mouth in the eastern Gulf of Ancud (Figs. 6, 7). Euphotic depth was 23 m near the head of the fjord but ranged from 30 to 33 m throughout the rest of the fjord (Fig. 6). Thus, subpycnal waters represented the lower 2/3 of the euphotic zone, whereas NO_x-rich conditions occurred in only the lower half of the euphotic zone.

Reñihue Fjord had the largest dawn-dusk variability in DO and pCO_2 and the highest depth-integrated chl-a among the fjords (Figs. 6, 7). Maximal chl-a occurred in the open region toward the mouth of the fjord and corresponded to a clear biological DO source and pCO_2 sink (Fig. 7). Other deviations from conservative mixing occurred where salinities increased near the fjord head and some shorelines. These alternative mixing relationships appeared to be linked to local upwelling, but at a much smaller scale than in Reloncaví Fjord. The consistent decrease in DO with depth despite relatively high chl-a was indicative of strong vertical mixing within the euphotic layer (Fig. 6). Notably, the euphotic depth was deeper (25–26.5 m) toward the head of the fjord where less saline surface waters originated from the Reñihue River compared to the euphotic depth in the middle-lower fjord (20.5–24 m), where brackish surface waters may have been more strongly influenced by waters flowing south from the Gulf of Ancud (Fig. 6).

3.5. Metabolism

3.5.1. GPP, R and NEP in surface waters

Surface waters in Reloncaví Fjord were net heterotrophic in the central section of the fjord (~23–33 km), where salinities of < 6 were maintained by freshwater input from the Puelo River (Fig. 8). As salinity increased in the upper Reloncaví, i.e, moving from the Puelo River toward the head of the fjord, GPP increased by a factor of three whereas R showed minimal variation. NEP reached 6.5 μmol-C kg^{-1} d^{-1} in this nutrient rich region where waters from depth were upwelled and mixed with riverine input. In lower Reloncaví, GPP showed a more moderate increase with salinity, i.e., moving from the Puelo River toward the mouth of the fjord, while R initially decreased (Fig. 8). Maximal NEP of 3.7 μmol-C kg^{-1} d^{-1} occurred about 10 km from the Puelo River, after which surface waters gradually transitioned to weak net heterotrophic

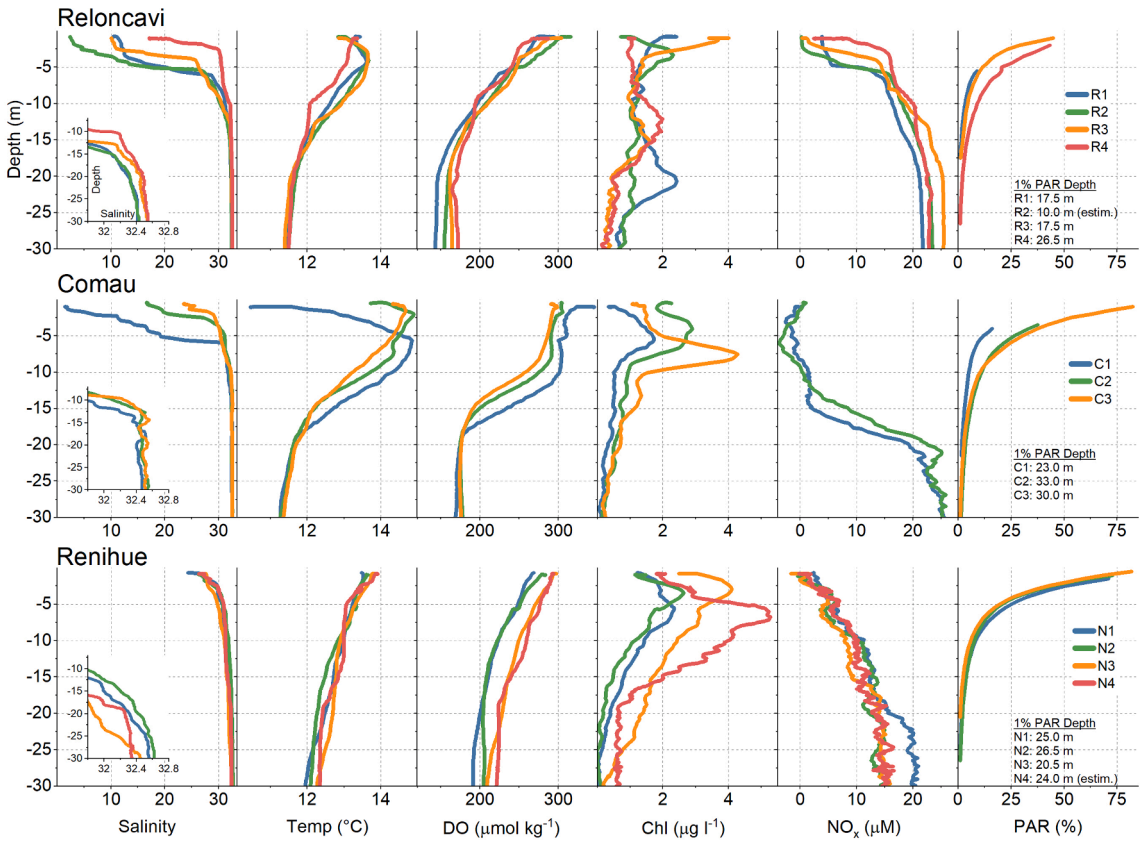

Fig. 6. Depth profiles at cast stations (Fig. 1) conducted between dawn-dusk surveys. Inset on salinity panel shows increased resolution at higher salinity values, particularly in Comau where inverse density stratification was observed. PAR profiles from stations R2 and N4 were projected based on the salinity:K_d relationship in the respective fjord, as these two stations were profiled after dark.

conditions near the fjord mouth due to a rapid increase in R.

Metabolic parameters in Comau showed a similar range and along-axis trend compared to lower Reloncaví, but parallel trends of GPP and R in Comau indicated closer metabolic coupling (Fig. 8). GPP and R were both negligible in fresh waters near the head of the fjord. As riverine and fjordic waters mixed within the first few km, GPP increased to its maximal value and NEP reached 7.2 µmol-C kg^{-1} d^{-1}. GPP then gradually decreased with increasing salinity until surface waters approached metabolic balance near the fjord mouth (Fig. 8).

Metabolic rates in Reñihue were up to four times higher than in the other two fjords, and the entire survey area of Reñihue was net heterotrophic despite high PAR during the survey interval (Figs. 3, 8). Notably, the narrow region within 5 km of the fjord head was net heterotrophic during both day and night. The negative GPP value in Fig. 8 indicates that the actual daytime R signal was higher than the GPP minus the estimated R in Eqs. (5)–(6). Metabolic rates were much higher in broader regions of the fjord, where peak values corresponded to maximal surface- and depth-integrated chl-a (Figs. 8-9). This region exhibited strong net heterotrophy, with NEP ranging from −5.1 to −13.4 µmol-C kg^{-1} d^{-1}.

3.5.2. *Primary productivity model and vertically integrated GPP (PP_I)*

Three data groups were identified for fitting PE curves based on initial assessment of depth-integrated irradiance and GPP in surface waters (Fig. 9a, Table S1). The first group (A) with the highest photosynthetic efficiency and maximum photosynthetic capacity ($\alpha = 0.176$, $P^b_{max} = 10.43$) consisted of nutrient rich regions in upper Reloncaví and Reñihue that were dominated by upwelling or vertical mixing. Photosynthetic parameters were considerably lower in a second group (B) ($\alpha = 0.086$, $P^b_{max} = 4.89$), which was characterized by nutrient deplete conditions (Fig. 8a, Table S1). This group included most of the Comau and the seaward region in Reñihue, where low NO_x at dusk indicated potential nutrient limitation (Fig. 7). A third group (C) with the lowest α and P^b_{max} ($\alpha = 0.050$, $P^b_{max} = 2.18$) included the regions of all three fjords that were most influenced by river input. These low salinity waters typically had high light attenuation (Fig. S6) and low nutrients (Fig. 7, Table S1), nonetheless, these conditions could not explain the similar PE relationship between the three fjords. Instead, the α and P^b_{max} in river-dominated surface waters may be more strongly influenced by planktonic community composition. Photopigment analysis of surface waters (see Clementson et al., 2020) indicated the dominance of diatoms at low salinity stations in each fjord, presumably due to high silicic acid input from rivers (e.g., Pérez-Santos et al., 2021). Fucoxanthin, which is indicative of diatoms, accounted for 70 % ± 27 % of the total photopigments in these samples. A more mixed phytoplankton community (19 % ± 14 % fucoxanthin) was observed at all other stations in the three fjords and throughout the CIS (Clementson et al. 2020), which is consistent with prior work in the region (Pérez-Santos et al., 2021).

Trends in PP_I estimates for March-April were generally similar to those in surface GPP measured during dawn-dusk surveys. Minimal PP_I occurred near the river mouths where light was most limited, particularly in subpycnal waters of Reloncaví and Comau (Fig. 9b). PP_I then increased as K_d decreased at stations with more saline surface waters; however, the relative contribution of surface and subpycnal waters to PP_I was dependent on local conditions. Surface PP_I was highest at nutrient-rich stations (R1, N3) while mid-layer and subpycnal PP_I was highest at stations where the surface layer of EW was nutrient deplete (R3, C2, C3, N4) or shallow (N1, N2) (Fig. 9b). PP_I in Comau (C2, C3) was higher than in Reloncaví (R1, *R*3) despite that most of the euphotic zone in Comau was nutrient deplete. PP_I appears to reach a similar maximum (or dynamic equilibrium) in regions with long residence times (C2, C3, R1, R4) and either nutrient or light limitation. The most

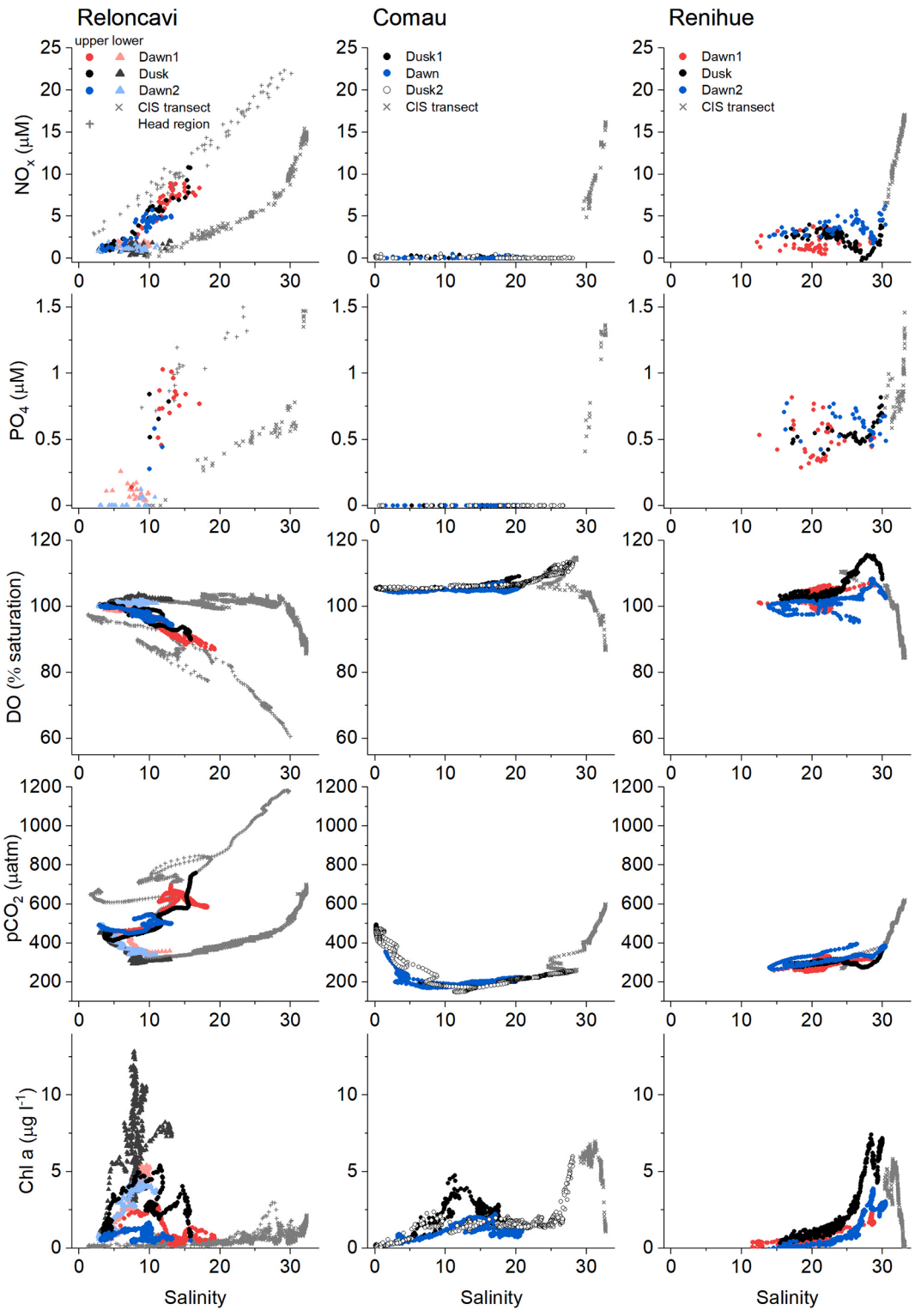

Fig. 7. Surface nutrients, DO, pCO_2, and chl-a measured during dawn-dusk surveys and transects from the fjord mouths toward higher salinities in the eastern Chiloe Sea (Fig. 1). See Fig. S5 for DO shown as μmol kg^{-1}.

apparent difference between fjords was that PP_I in Reñihue (1.7–3.5 g-C m^{-2} d^{-1}) was 2–3 times higher than in Reloncaví and Comau, even at station R4 which was outside of the Reloncaví Fjord mouth.

A key function of the productivity model was to translate free-water metabolic rates into areal rates (g-C m^{-2} d^{-1}), which enabled more direct comparison with metabolic data in available literature. Reloncaví Fjord is the best resolved fjord among the three study systems in terms of seasonal variability, and results from this study support the seasonal patterns identified in prior studies. PP_I in Reloncaví Fjord (0.3–1.7 g-C m^{-2} d^{-1}) in March (Fig. 9) fell between PP_I values previous reported in the same fjord for winter/autumn (<1 g-C m^{-2} d^{-1}) and summer/spring (1–6 g-C m^{-2} d^{-1}) (González et al., 2011; Montero et al., 2011). A simple average of seasonal data from this and prior studies yields an annual PP_I of ~4.3 g-C m^{-2} yr^{-1}, which would place Reloncaví Fjord in the top

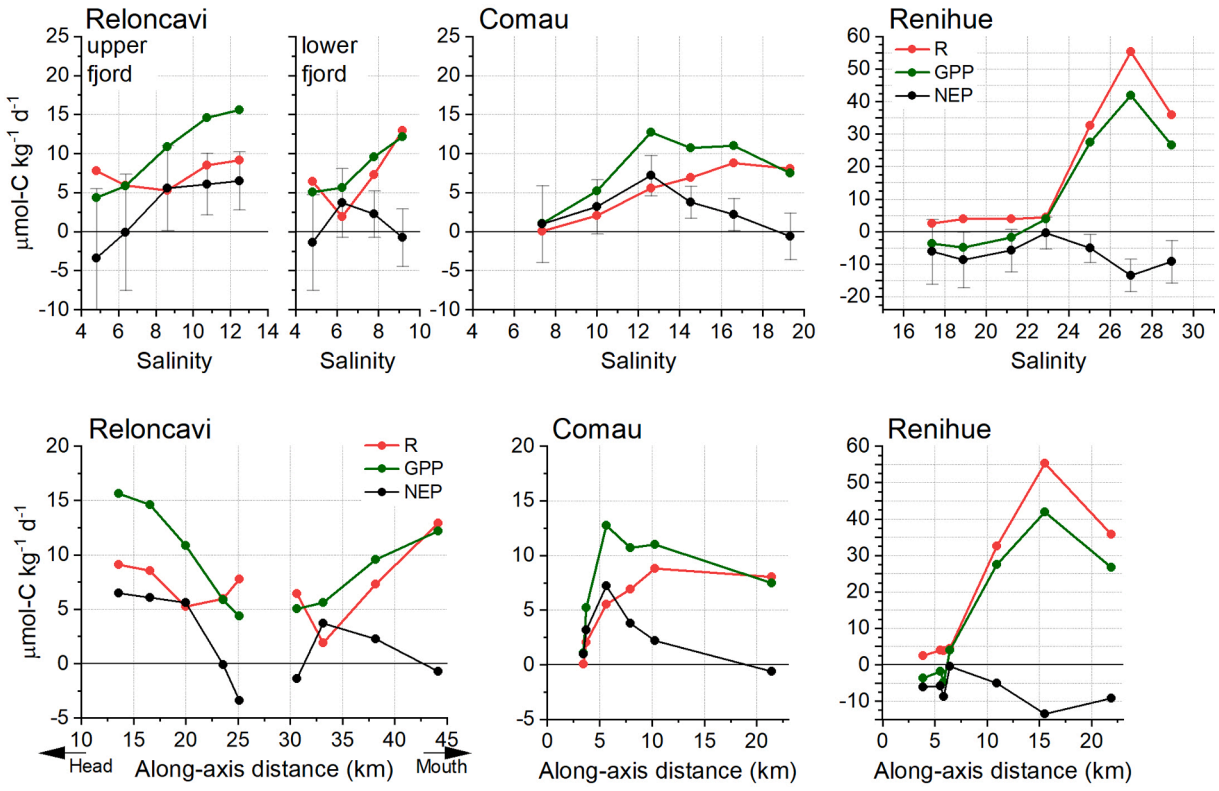

Fig. 8. Metabolic parameters vs salinity (top) and along-axis distance (bottom) for binned underway data. Positive NEP values indicate net autotrophy. For simplicity, error bars are shown only in the top panel for NEP. GPP and R are subject to the same error range as NEP for each respective bin.

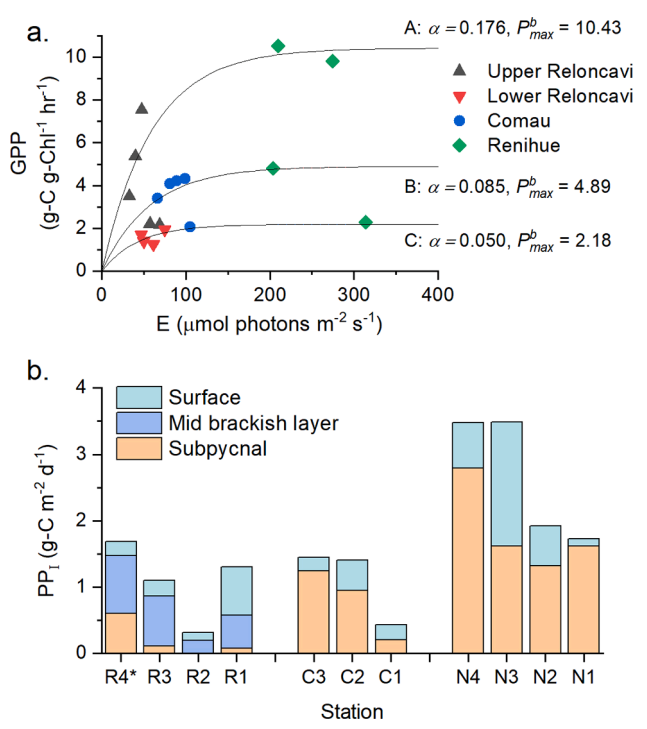

Fig. 9. a) Terms for the primary productivity model in Eqs. (10)–(11) fit to surface GPP (Fig. 8) for three data groups* (A,B,C), and **b)** depth-integrated results obtained by applying these terms to vertical profile data (Fig. 6) and using daily averaged PAR at Huinay Research Station from 9 March to 8 April 2018. *See Table S1 for summary data corresponding to points in panel a.

~20% of estuarine-coastal ecosystems compiled in a global review by Cloern et al. (2014). PP_I in Comau Fjord (1.4 g-C m^{-2} d^{-1}) was also within values previously observed in the fjord (1–3 g-C m^{-2} d^{-1}; Aracena et al., 2011; Iriarte et al., 2013), although seasonal variability has not been well resolved. Productivity has not been previously documented in Reñihue Fjord. However, prior data from within Northern Patagonia confirmed that the high PP_I observed in Reñihue Fjord was indeed realistic. For example, PP_I of 3.5 g-C m^{-2} d^{-1} in Reñihue was within PP_I ranges reported near the Desertores Islands (González et al., 2010) and in other Patagonian fjords in the region, such as Puyuhuapi Fjord and Aysén Fjord (1–5 g-C m^{-2} d^{-1}; Aracena et al., 2011; González et al., 2011; Daneri et al., 2012; Montero et al., 2017).

3.6. Density structure and circulation

3.6.1. Double-diffusive convection

Vertical mixing regimes were examined using the Turner angle, which accounts for vertical instability due to differential diffusion rates of heat and salt. Below, we briefly define each regime and describe where it was observed in the study region. Only *Tu* values within the double diffusive range (-90° to 90°) are considered, as values outside of this range reflect instability that is rapidly resolved by top-heavy convection. While some *Tu* values from underway profiles were in this unstable range or were otherwise outliers, comparison with *Tu* from discrete profiles suggest that these outliers were an artifact of rapid profiling speed (Fig. 10). This greater noise in underway *Tu* data was expected given that the much faster profiling speed of the underway CTD made it more prone to sensor hysteresis and potentially cavitation, particularly as the CTD reached the maximum depth and began to ascend.

The ***diffusive layering regime*** (-90° $< Tu <$ -45°) develops when colder, fresher water covers warmer, saline water. Weak diffusive layering occurred in surface waters of about 0 to 5 m depth in all fjords, as all riverine input was colder than ambient fjord water (Figs. 5, 10).

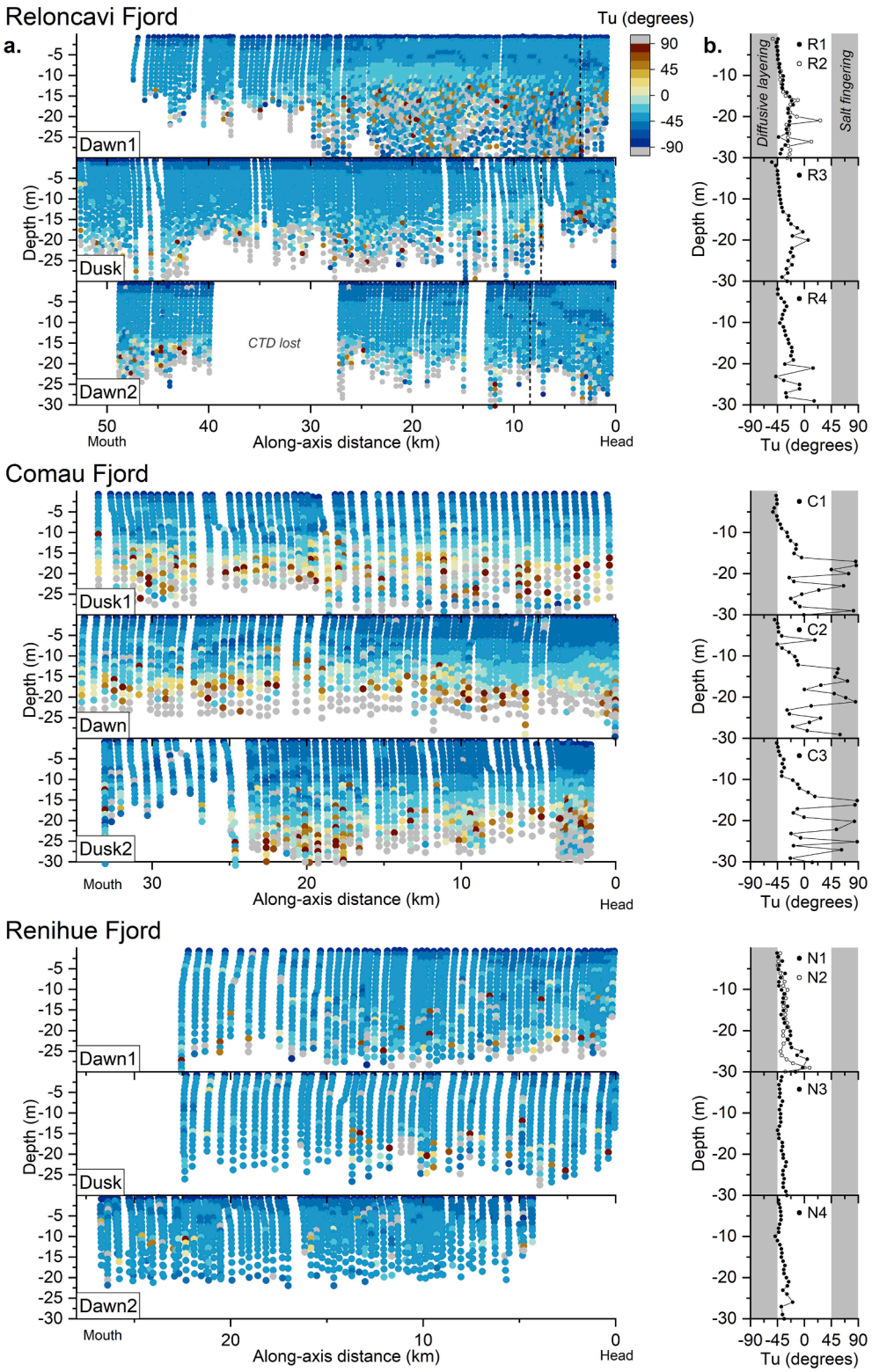

Fig. 10. Depth profiles of Turner Angles based on **a)** underway CTD profiles and **b)** CTD cage casts at discrete profiling stations showing three regimes of double diffusive convection during dawn-dusk surveys. Comparison between underway profiles and cage casts suggest outliers (grey values) in underway data were artifacts of rapid profiling speed.

Cooler surface waters were then maintained throughout the study region by meteorological conditions that favored heat loss to the atmosphere.

The ***double stable regime*** (-45° $<Tu<$ 45°) develops when warmer, fresher water covers colder, saline water. Double stability was the dominant condition in Reloncaví and Reñihue Fjords (Figs. 4, 5, 10), as both temperature and salinity decreased from 5 to 50 m depths.

The ***salt fingering regime*** (45° $<Tu<$ 90°) develops when warmer, more saline water covers colder, less saline water. Salt fingering occurred throughout Comau at depths from 15 to 30 m and was confirmed by both underway and discrete CTD data (Figs. 5, 10). The

mechanism by which salt fingering develops in Comau and relevant implications are discussed in Section 4.2.

3.6.2. Rotational dynamics

The Rossby radius in Reloncaví and Comau ranged from 3 to 9 km and was always higher than the width of the fjord (Fig. 11). These length scales indicate that rotational effects are minor relative to along-axis flow. The L_R/w ratios throughout Reloncaví and Comau were consistent with narrow mid-latitude fjords that have conventionally been reduced to two-dimensional systems when considering advective exchange (Cottier et al., 2010). The shorter L_R in Reñihue and wider mouth led to a L_R/w < 1, which was about 5 times lower than the other two fjords (Fig. 11). Based on this length scale, Reñihue can be classified as a 'broad' fjord where baroclinic flows are influenced by rotational dynamics (Cottier et al., 2010). The rotational characteristics of the three fjords implied by the Rossby radius were generally consistent with observed trends in across-axis variability (Section 3.2) and showed good agreement with the Los Lagos Model (Supplemental M1, M2).

3.6.3. Hydrodynamic model

Velocity profiles for March 2018 were extracted from the Los Lagos Model in order to characterize circulation in the three fjords. The model does not resolve local topographic influence on winds that have been identified as important forcing mechanisms in prior fjord studies (e.g., Skogseth et al., 2007). Accordingly, Los Lagos Model data are presented for comparison between fjords and analysis of general trends rather than assessment of time-resolved velocities. The major differences between and within fjords are summarized in the following paragraphs along with a first-order assessment of model trends based on observational data.

Reloncaví showed large variability along the fjord axis due to the central location of the major riverine input (Fig. 12). Strong seaward velocities in two surface layers near the fjord mouth were balanced by landward flow at mid-depths (30–100 m) (Fig. S7). Modelled velocity profiles showed an opposite trend in upper Reloncaví, where currents were landward in the surface layer and seaward at mid depths (Fig. 12).

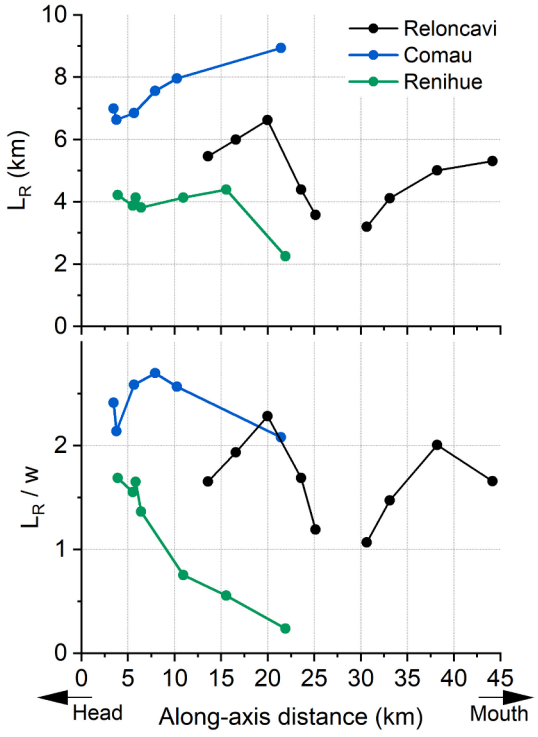

Fig. 11. Rossby radius (L_R) and fjord width (w) ratio in the three fjords.

Observed data were consistent with modelled velocities in lower Reloncaví. For example, the decreasing pycnocline depth near the mouth (Fig. 4) implied acceleration of seaward surface currents (e.g., Stigebrandt, 2012). The model-observation agreement was more equivocal in upper Reloncaví, as the upwelling observed on dawn-dusk surveys was not reflected in the Los Lagos Model, presumably due to the insufficient resolution of local-scale winds as noted above (Supplemental M1).

Current velocities in Comau were several times lower than in the other fjords and showed consistent along-axis circulation. Modelled surface velocities were landward, driven by up-fjord winds, while underlying currents down to ~70 m depth were seaward (Figs. 12, S7). However, the modelled surface layer was more saline (salinity: 24–26) than observed conditions and showed a more gradual salinity increase with depth rather than distinct density layering (Fig. 4), which likely affected the simulation of wind forcing on surface flow, as discussed in Section 4.2.1.

Current velocities in Reñihue were the highest and most variable among the three fjords (Fig. 12). The predominant current direction shifted several times between 0 and 30 m depth while both the absolute and average velocities remained high. Modelled surface currents at the three along-axis sites in Fig. 12 were landward, but unlike in Comau, the direction of surface currents varied across the axis of Reñihue fjord. Landward surface currents along the northern shoreline transitioned to seaward currents along the southern shoreline (Supplemental M2). Analysis of temporal trends confirmed a clear influence of Coriolis and episodic wind forcing on surface currents, and spatial surveys confirmed large across-axis gradients throughout the fjord.

4. Discussion

The comparison of three fjords under similar seasonal conditions using consistent observational methods enables resolution of key functional differences between these study systems. This understanding includes how large-scale forcing factors such as seasonal and synoptic climate-ocean processes interact with local scale morphology to control physical dynamics in fjords. These physical processes in turn influence metabolic function in fjords, which have previously been linked to variable drivers ranging from seasonal light cycles (Iriarte and González, 2008) to more complex interactions between wind forcing, river input and larger-scale hydrodynamics in connected coastal waters (e.g., Aiken, 2012; Iriarte et al., 2014; Montero et al., 2017). The following sections examine physical processes and metabolic controls in each fjord individually, noting key comparisons between fjords and connectivity within the CIS. The context of this discussion is generally constrained to the seasonal conditions during the study period, which represent the typical transition from summer to autumn marked by an increase in river discharge (Fig. 2), a decrease in sea surface temperature (Saldías et al., 2021) and a shift to overall dominance of northerly winds amid passage of high and low atmospheric pressure systems (Pérez-Santos et al., 2019).

4.1. Reloncaví fjord

4.1.1. Dominant geophysical forcing

In Reloncaví Fjord, the Puelo River mouth and the approximate 90° turn in the middle of the fjord represent the boundary where the dominant drivers transition between the upper and lower fjord. Upwelling observed in upper Reloncaví (Fig. 4) supports the major role of synoptic-scale wind forcing reported in prior studies. Valle-Levinson et al. (2007) and Castillo et al. (2017) observed a wind-driven seiche with a period of ~3 days in Reloncaví Fjord and estimated that seiche-driven mixing may be comparable to tidal forcing. Given the geomorphology of Reloncaví Fjord, it would be expected that mixing driven by these barotropic exchanges would be concentrated in the upper fjord. That is, the absence of a sill and the decreasing depth toward the fjord

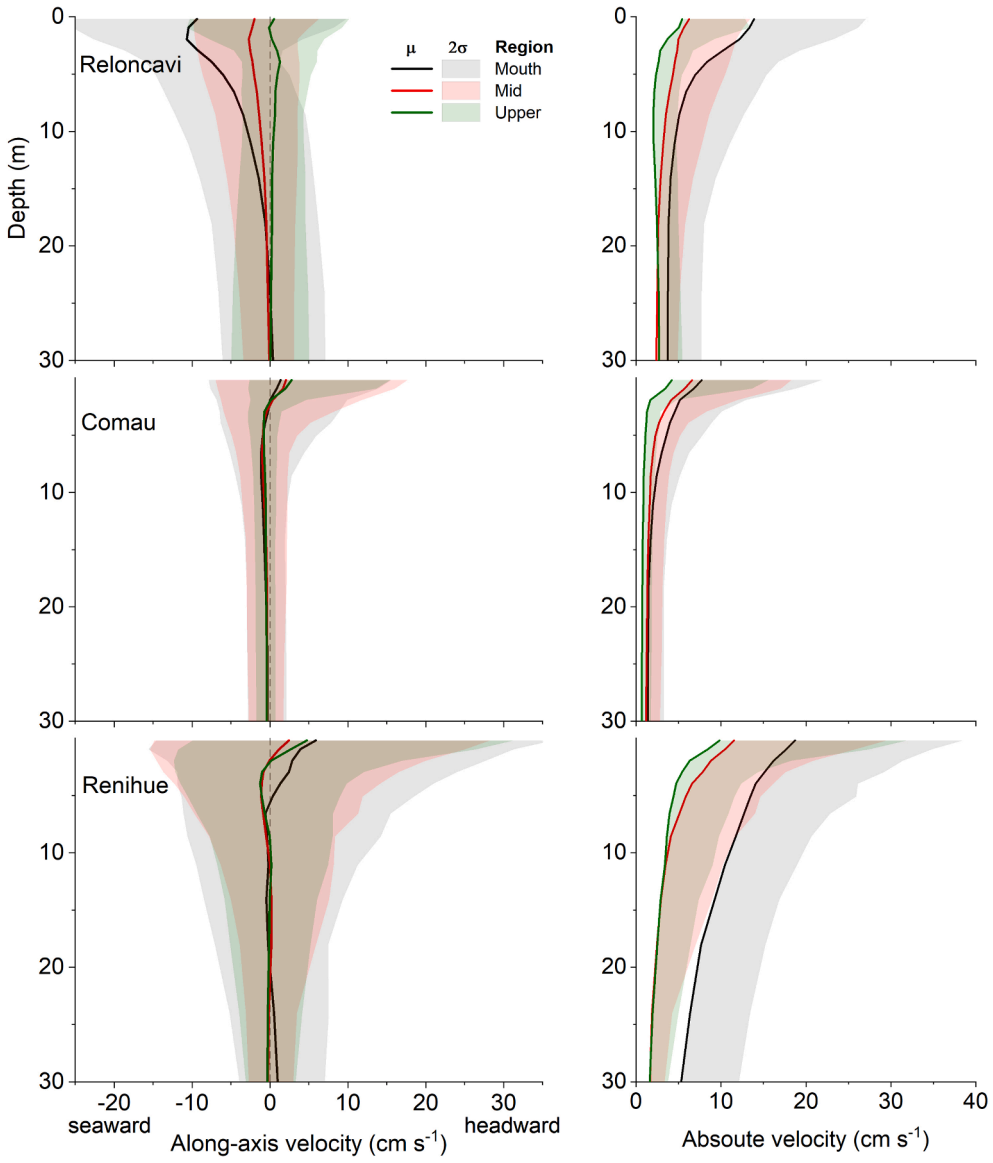

Fig. 12. Velocity profiles from the Los Lagos Model at three locations (Fig. 1) along the axis of each fjord. See Fig. S7 for profiles from 0 to 100 m depth.

head imply that dissipation of seiche and tidal energy is most likely to occur during wave reflection in the upper fjord (e.g., Arneborg and Liljebladh, 2001). This energy dissipation may also be enhanced by the location of the main riverine input, the Puelo River, at the transition from the upper to the lower fjord. That is, surface water mixing due to down-fjord winds weakens the pycnocline in the upper fjord, which in turn dampens internal wave energy through direct diapycnal mixing (Fig. 13) (e.g., Baines, 1982). While barotropic current velocities would be maximal at the seiche node in the lower fjord (Castillo et al., 2017), diapycnal mixing would be minimized due to strong stratification. This mechanism would explain the two seaward-flowing surface layers observed during down-fjord winds in this study, the Los Lagos Model (Fig. 12) and by Castillo et al. (2012). The overall result is that kinetic energy in barotropic flows is converted to potential energy through mixing in the upper fjord. This mixing generates an along-fjord density gradient which drives seaward baroclinic flow of a brackish layer (~12–28 salinity at 5–12 m depth) underlying the fresher seaward-flowing EW layer in the lower fjord (Fig. 13). These active mixing processes lead to a stable density profile in the vertical such that there is no potential for double-diffusive processes to occur (Fig. 10).

4.1.2. Controls on metabolism in Reloncaví: River input and wind-driven upwelling/circulation

River discharge is the dominant forcing mechanism in Reloncaví, but the mid-fjord location of the Puelo River mouth also amplifies the role of synoptic winds in regulating circulation and metabolic functioning. Metabolic controls are most easily understood following hydrodynamic flow, starting at the marine end member, Reloncaví Sound. The subpycnal chl-a maximum observed in Reloncaví Sound was preserved in the landward flowing layer (depth > 13 m) near the mouth of Reloncaví Fjord (Fig. 6). GPP in these bottom waters was limited by light attenuation in the two overlying layers (Fig. 6), and the low productivity relative to timescales of physical transport resulted in a more mixed vertical distribution of chl-a as this layer flowed up-fjord. In the upper fjord, upwelling and mixing driven by down-fjord winds and resultant internal waves brought nutrient-rich waters into the euphotic layer, triggering the highest GPP and NEP observed within the system (Figs. 8, 9, 13, Table S1). Here, the presence of a deep chl-a maximum at the lower boundary of the mixing layers (Fig. 6) combined with temporal variability observed in the pycnocline depth (Fig. 4) suggest that a relevant portion of PP_I may occur in nutrient-rich waters that are only periodically in euphotic zone during upwelling events. This bimodal

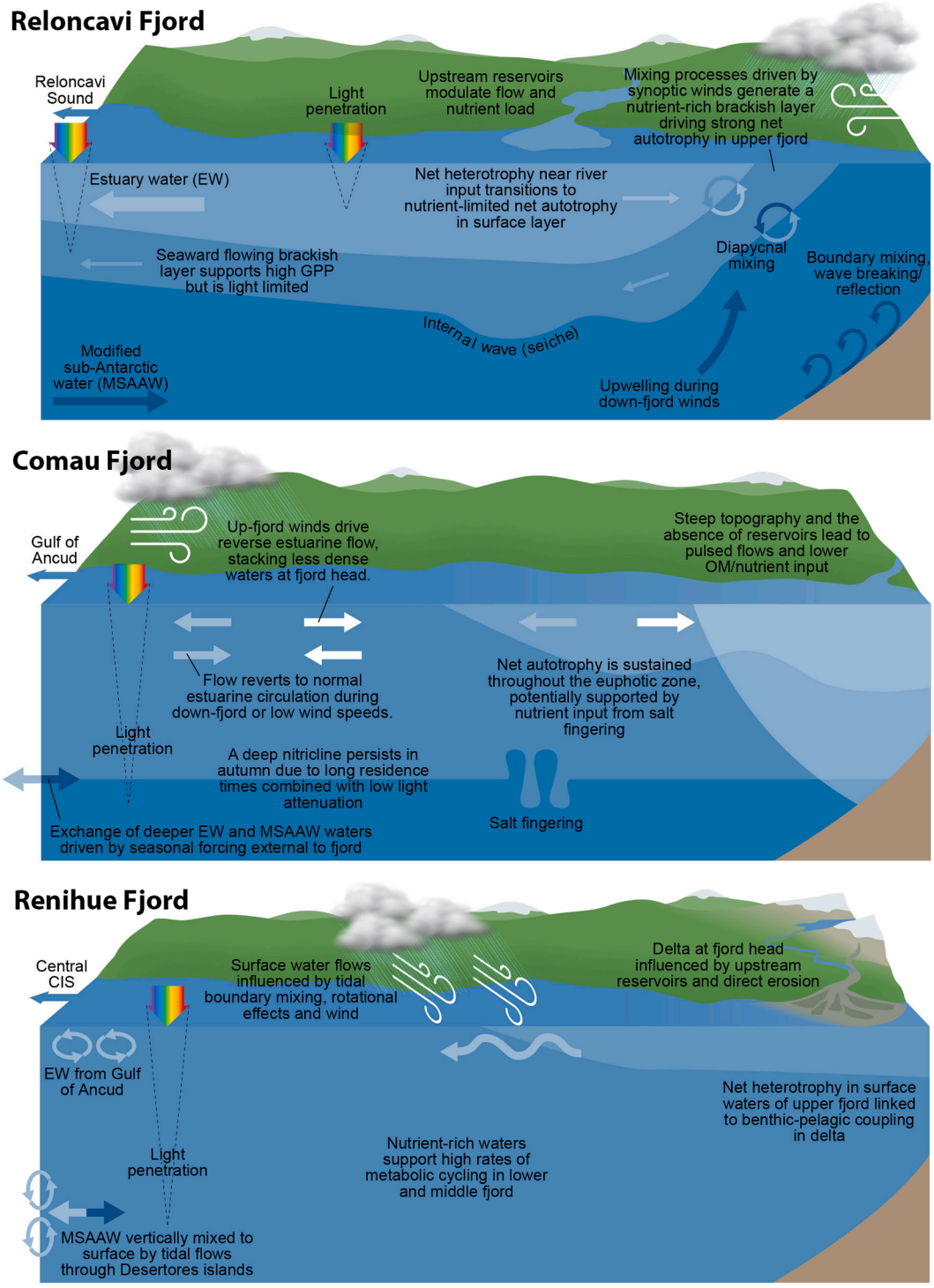

Fig. 13. Conceptual diagram showing how typical environmental forcing in late summer-autumn interacts with local morphology to control physical dynamics and in turn influence metabolic function in the three northernmost fjords in Patagonia.

distribution of chl-a with depth may reflect partitioning of phytoplankton community composition due to nutrient and light requirements along with motility (e.g., Montero et al., 2017; Pérez-Santos et al., 2021), and it also implies different fates for planktonic OC generated near the surface compared to near the deep chl-a maximum. That is, autochthonous OC produced at depth may be retained in the upper fjord whereas autochthonous OC in surface waters is more likely to be advected seaward as these brackish waters are subducted under less saline waters over wind and tidal cycles (e.g., Fig. 13, Supplemental M1).

Near the Puelo River mouth, low surface nutrients, light limitation, and elevated terrestrial organic matter explain the net heterotrophy and the low GPP and PP_I in both surface and intermediate brackish layers (Figs. 8-9, Table S1). Uptake of remaining nutrients in the surface layer explains the transition to net autotrophy and then back to net heterotrophy moving from the river toward the fjord mouth (Fig. 8). Unlike surface waters, the underlying brackish layer remained nutrient rich, which would support the high PP_I that was estimated in the lower fjord

(Fig. 9b, 13). Although respiration was not measured in this layer, the persistence of nutrient-rich conditions as well as O_2 values < 100% saturation, indicated that the intermediate water layer was light-limited and not strongly autotrophic.

The influence of synoptic winds and topography imparts an important control on hydrodynamics and thereby metabolism in Reloncaví, and similar upwelling processes have been observed in other fjords. The role of wind forcing in controlling blooms has also been confirmed in New Zealand and northern hemisphere fjords (Lindahl et al., 1998; Goebel et al., 2005; Collins et al., 2009). For example, PP_I in the upper Reloncaví (1.3 g-C m^{-2} d^{-1}) was similar to that observed in Puyuhuapi Fjord by Montero et al. (2017) (0.6–1.6 g-C m^{-2} d^{-1}), where the authors linked a winter phytoplankton bloom with a bimodal vertical distribution of chl-a to wind-driven mixing during passage of a low atmospheric pressure system. Although PP_I estimates herein were subject to moderate uncertainty, e.g., due to productivity model assumptions and temporal scaling based on PAR data, PP_I estimates were consistent with seasonal trends in prior studies (Section 3.5.2). Moreover, it is clear that GPP and NEP were closely linked to hydrodynamic processes controlled by seasonal drivers. The conditions during this study are typical for the last months of the productive season (March - May). Higher riverine discharge and up-fjord winds that are typical earlier in the productive season (austral spring) would likely lead to two-layer circulation in the euphotic zone, where maximal productivity and chl-a occur in the landward flowing subpycnal layer (Castillo et al., 2012). These seasonal drivers can vary over annual and longer timescales (Narváez et al., 2019; Pérez-Santos et al., 2021; Saldías et al., 2021). Iriarte et al. (2017) found that autumn phytoplankton blooms of > 2 μg chl-a l^{-1} in Reloncaví were generally associated with Puelo River discharge < 350 m^3 s^{-1}. During this study, riverine input was low (~250 m^3 s^{-1}) such that strong stratification was maintained in the lower fjord, while down-fjord winds and resultant internal waves were sufficient to mix waters toward the head, thereby leading to nutrient rich conditions. Similar wind-driven forcing was observed in Reloncaví during low discharge by León-Muñoz et al. (2013) and Valle-Levinson et al. (2007). During years of higher discharge, strong stratification can persist throughout the entire fjord in autumn, thereby limiting vertical mixing and nutrient availability in the euphotic layer. For example, Montero et al. (2011) found low GPP and net heterotrophic conditions throughout Reloncaví Fjord in autumn 2009, when Puelo River discharge was > 500 m^3 s^{-1} and a low salinity, nutrient deplete surface layer occurred throughout the fjord.

4.2. Comau fjord

4.2.1. Dominant geophysical forcing

Synoptic winds were also a major forcing mechanism in Comau, influenced by the fjord geomorphology. Meteorological observations near Huinay (Fig S2; Sepúlveda-Steiner et al., 2015; Reche et al., 2021) show that during weak synoptic forcing, winds are dominated by a katabatic sea breeze, with the direction and magnitude largely controlled by the local topography. This sea breeze diminishes under strong synoptic winds, and Comau's narrow funnel that opens to the north makes the fjord particularly exposed to northerly winds during low atmospheric pressure systems. Sustained up-fjord winds have been shown to induce seaward flow in an intermediate layer beneath the wind-driven landward flow in the surface layer of fjords (Inall and Gillibrand, 2010; Moffat, 2014), and the Los Lagos Model indicated that this reverse estuarine circulation was dominant in Comau surface waters during March 2018 (Figs. 12, 13). Barotropic reverse flow during northerly winds has also been confirmed by observations in Comau, including a two-week hydrodynamic study by Sepúlveda-Steiner et al. (2015) and current velocity data from aquaculture impact assessments (Fig. S8). Because increased rainfall often accompanies northerly winds during low atmospheric pressure systems, baroclinic forcing from high freshwater input can re-establish estuarine circulation despite northerly winds. However, current velocity data from prior studies, combined with dawn-dusk surveys from this study (Figs. 4, 5), suggest that seaward surface flow during northerly winds in Comau occurs as a brief pulse of freshwater out of the system rather than as a sustained flow. These episodic flows in Comau are likely due in part to the lack of a hydrological reservoir, i.e., upstream lakes on the main riverine input such as those in Reloncaví and Reñihue Fjords, which would act as a buffer supporting more steady flow.

Local wind and riverine forcing alone would not easily explain the thermohaline layering indicative of salt fingering that was observed at 15–25 m throughout Comau Fjord (Figs. 6, 10). This layer represents MSAAW that is influenced by interaction with overlying EW as well as larger-scale exchange mechanisms in underlying and adjoining waters. Subpycnal layers with similar characteristics have been observed in several other Chilean and global fjord systems in which horizontal exchange of bottom waters has been linked to density structure external to the fjord itself, particularly in fjords like Comau that lack a shallow sill (Aiken, 2012; Pinilla et al., 2020). Several lines of evidence support this external control on MSAAW exchange and density structure in Comau. First, vertical profiles during a transect of the Gulf of Ancud on 26 March 2018 showed thermohaline layering at depth that was similar to that observed in Comau. This inverse salinity stratification in the Gulf of Ancud during March 2018 was also reflected in the South-Austral Operational Model (Ruiz et al., 2021) and briefly in the Los Lagos Model. Second, the low NO_x from 0 to 20 m depth indicates that the high salinity layers within this range are unlikely to originate from local upwelling. Instead, these waters are more likely to be transported from the Gulf of Ancud (Fig. 13), where nutrients can be depleted from high salinity layers that remain within the euphotic zone. Finally, analysis of vertical profiles compiled from prior datasets (Müller, 2012; Fillinger and Richter, 2013; Laudien et al., 2014; Laudien et al., 2017a,b), suggests that density structure conducive to salt fingering is a seasonal feature of Comau and proximal waters in the Gulf of Ancud (Fig. S9).

4.2.2. Controls on metabolism in Comau: wind-driven circulation, connectivity to the catchment and CIS, and salt fingering

Comau had the most nutrient-deplete surface waters and the deepest nitricline among all regions of the CIS. These conditions were consistent with prior observations in Comau during summer and autumn (Mayr et al., 2011; Iriarte et al., 2013; Olsen et al., 2014, Olsen et al., 2017) as well as with modelling results that show Comau surface waters have the longest residence time in the Los Lagos Model domain (Gorton et al., 2018). Water column profiles in February – April, which are available from four prior years (Müller, 2012; Fillinger and Richter, 2013; Laudien et al., 2014; Laudien et al., 2017a,b), generally showed conditions that were similar to those observed in this study; an oxycline and presumably nitricline at 15–25 m. Unlike Reloncaví Fjord, the aforementioned historical data showed no apparent interannual trend between river discharge and biological parameters (DO and chl-a) in Comau Fjord.

Long transport times relative to timescales of biological activity, combined with low light attenuation, contribute to the deeper nitricline in Comau relative to other fjords; the average euphotic depth in Comau (28 m) was the deepest among the three fjords and was twice as deep as in Reloncaví Fjord (14 m). However, nutrient-deplete conditions in Comau are also influenced by surface conditions in the Gulf of Ancud and in turn the northeastern CIS. These conditions depend on freshwater input from the Puelo River over the preceding weeks and months combined with wind and frictional forcing as well as larger scale climate-ocean processes (Narváez et al., 2019; Pérez-Santos et al., 2021; Saldías et al., 2021). Discharge from the Puelo River into Reloncaví Fjord and Sound forms a surface layer of EW that then flows south through the central Gulf of Ancud before deflecting eastward around the Desertores Islands and continuing southward along the eastern CIS margin (Herzfeld, 2018; Ruiz et al., 2021). Passive tracer results from the Los Lagos Model have shown that some of these buoyant surface waters are entrained in an eddy that persists across the eastern Gulf of Ancud (Herzfeld, 2018). Continuous surface sampling and vertical profiles

during a transect through this eddy on 26 March 2018 showed nutrient deplete conditions similar to those in Comau (Crosswell, 2018). It follows that nutrient availability as well as planktonic composition and biomass in Comau may be linked to larger scale processes in the CIS. For example, Sepúlveda-Steiner et al. (2015) observed a rapid increase in chl-a centered at a depth of ~15 m in Comau Fjord during a storm event in January 2014. The authors attributed this increase to advection of phytoplankton from the Gulf of Ancud due to wind-drive forcing. Thus, physical dynamics and metabolic activity in Comau appears to be coupled to processes in the eastern Gulf of Ancud over synoptic to seasonal scales with longer-term impacts on the fate of autochthonous OC. Supporting this, Silva et al. (2011) found that sediments in Comau were dominated by marine material and were nearly identical to those in the eastern Gulf of Ancud. By contrast, sediment in Reloncaví Fjord were dominated by terrestrial material from the Puelo River.

Metabolic parameters in Comau surface waters showed similar magnitudes and along-axis trends as the lower Reloncaví; the main difference was low metabolic rates and slight net autotrophy in river-dominated waters at the head of Comau Fjord (Fig. 8). Samples at the mouth of the Vodudahue River (Fig. 1) collected between dawn-dusk surveys were characteristic of rainwater (TA = 18 μmol kg^{-1}; NO_x and PO_4 = below detection), reflecting short freshwater residence time in the catchment due to steep topography and the lack of a hydrological reservoir. By comparison, samples at the mouth of the Puelo River in Reloncaví showed a greater rock weathering signature (TA = 229 μmol kg^{-1}; NO_x = 0.3 μM; PO_4 = below detection), reflecting longer freshwater residence times in several large upstream lakes of the Puelo catchment. The negligible nutrient and organic matter content of rain-like river water in Comau would explain the near absence of metabolic activity at low salinities and also the low K_d, particularly at salinities<25. These nutrient deplete, optically clear surface waters also explain why subpycnal waters represented the greatest portion of water column PP_I in Comau relative to the other study systems (Fig. 9, Table S1). Both the K_d and PP_I from this study (0.10–0.41 m^{-1}, 0.4–1.4 g-C m^{-2} d^{-1}, respectively) (Figs. 9, S6) were consistent with a microcosm study in Comau by Iriarte et al. (2013), who reported K_d = 0.24–0.31 and GPP = 1–3 g-C m^{-2} d^{-1}. The authors also found that most GPP occurred in subpycnal waters and noted that the slow biological response to nutrient additions (4–8 days) may be linked to the "storage hypothesis", whereby phytoplankton are acclimated to brief pulses of nutrients in vertically stratified environments.

With minimal nutrient input from either rivers or surface-water exchange with the Gulf of Ancud, deep waters within Comau represent the main source of nutrients to surface waters during late summer. However, availability of these nutrients for primary production depends on vertical transport processes. Modelling results from Sepúlveda-Steiner et al. (2015) suggest that wind-driven mixing of deeper waters only occurs during intense storm events, as wind energy is dissipated within the euphotic zone during calm conditions. Thus, given the negligible or episodic nutrient loads from other sources, the salt fingering form of double diffusive convection observed in this study appears to be a significant mechanism for nutrient input to the euphotic zone in Comau (Fig. 13). While salt fingering has been reported in other fjords (Spear and Thomson, 2012; Pérez-Santos et al., 2014), this is the first time for which we are aware that it has been observed in the euphotic zone and implicated as a significant control on primary production.

4.3. Reñihue fjord

4.3.1. Dominant geophysical forcing

As a broad fjord with low riverine input, Reñihue is influenced by rotational effects that drive cross-axis variations in stratification and flow, and the vertical structure within the fjord is strongly impacted by the geomorphologic setting in the central CIS. Here, the Los Lagos Model shows that turbulent shear generated by tidal flow through the Desertores Islands produces vertical velocities that are significantly larger than in the Gulf of Ancud or Reloncaví Sound (Herzfeld, 2018; Ruiz et al., 2021). Mixing may also be enhanced within the fjord itself by eddies that are generated as along-shore tidal and geostrophic currents pass the headlands and seamounts in the lower fjord (Fig. 13, Supplemental M2). The Los Lagos Model does not resolve fine-scale wind forcing that has been shown to drive cyclonic surface currents and upwelling in broad fjords due to Ekman transport (Cushman-Roisin et al., 1994; Skogseth et al., 2007). However, due to the low riverine input in Reñihue, the potential displacement of the thin surface layer by synoptic or seasonal winds is likely to be of minor significance relative to the influence of tidal forcing. This dominance of tidal mixing is reflected in low seasonal variability in Reñihue; in a study of SST trends from 2003 to 2018, Narváez et al. (2019) found that the standard deviation in Reñihue (~2 °C) was about half that observed in Reloncaví and Comau fjords. The low Rossby term (L_R/w < 1) in Reñihue implies that geostrophic flows along with tidal and wind forcing will generally increase circulation and exchange. These internal processes combined with turbulent vertical mixing in the central CIS generate a doubly-stable density structure that precludes diffusive convection in Reñihue. Vertical profiles from this study as well as other available profile data (Crosswell, 2017; Laudien et al., 2017c) (Figs. 6, 10) confirm that Reñihue Fjord is the most vertically mixed and diffusively stable of the three northernmost Patagonian fjords (Fig. 13).

4.3.2. Controls on metabolism in Reñihue: Tidal mixing, connectivity to the central CIS, and benthic-pelagic coupling

Supply of nutrients from depth due to tidal mixing combined with fjord geomorphology supported metabolic rates in lower Reñihue (Figs. 6, 7, 13) that were among the highest reported in Patagonian fjords, even in nutrient enrichment studies (González et al., 2011; González et al., 2013; González et al., 2016; Montero et al., 2017; Saggiomo et al., 2011; Daneri et al., 2012; Iriarte et al., 2018). Mixing may have been enhanced by the occurrence of spring tides during the survey interval. However, available observational data suggest that Reñihue surface waters are consistently nutrient-rich (Crosswell, 2017; González et al., 2019), and remote sensing studies show high chl-a fluorescence year-round (Saldías et al., 2021; Vásquez et al., 2021). Moreover, the latter studies show elevated chl-a in Reñihue even when values are seasonally low in other fjords, which is presumably due to Reñihue's low riverine input combined with rapid mixing and flushing rates.

Of the three fjords, metabolic rates (GPP and R) in Reñihue were the most closely coupled (Fig. 8). It is plausible that the short timescale of nutrient replenishment from tidal forcing relative to timescales of biological activity could result in a dynamic equilibrium whereby planktonic metabolism is controlled primarily by light availability. It follows that more strongly stratified or lower energy fjords like Reloncaví and Comau would be more conducive to planktonic 'bloom and bust' cycles driven by seasonal and synoptic meteorological forcing in addition to light availability. Longer observational periods and/or integration with biogeochemical models will be required to support these generalizations and explore more complex controls on ecosystem function. For example, despite close coupling of GPP and R, Reñihue surface waters were the most net heterotrophic among the three fjords. This net heterotrophy may be persistent in the euphotic zone if nutrient input from depth is also accompanied by upward transport of labile organic matter. Alternatively, supersaturation of DO in surface waters (Fig. 7) combined with the low PAR during the dawn-dusk survey interval suggest that the lower Reñihue may be closer to metabolic balance over longer intervals that constrain average light and tidal conditions. Other factors that were not quantified in this study may also be important controls on metabolism in Reñihue, including top-down regulation by higher trophic levels. There was some anecdotal evidence for the role of grazers in the heterotrophic signal in Reñihue, as the most intense fish and seabird feeding during the entire research voyage was observed at mixing fronts within Reñihue Fjord.

While the upper Reñihue is relatively small, this region warrants

specific consideration given that it is the only study area where benthic processes may be directly couped to pelagic metabolism. The head of Reñihue Fjord is formed by shallow waters and intertidal regions of a tidal delta. This delta is the terminus of a braided channel that forms 20 km upstream where erosion from the Michinmahuida Volcano joins the Reñihue River, which flows from a series of lakes 10 km farther upstream (Fig. 13). Samples of riverine or low salinity waters were not possible due to the timing of dawn-dusk surveys. However, extrapolation of the TA trend from moderate salinities yields a freshwater endmember (TA = 301 μmol kg^{-1}) that, like in the Puelo River, is indicative of chemical weathering and long residence times in catchment lakes. While nutrients could not be similarly extrapolated to a freshwater endmember, it is reasonable to assume that riverine nutrient input in Reñihue is of minor significance due to the low river flow and nutrient-rich conditions throughout the water column in the fjord.

The upper Reñihue was the only study location that was net heterotrophic during the day. This may be due to the role of benthic respiration in the shallow waters and intertidal regions in upper Reñihue, which are several times larger than in the other study systems. The timing of dawn-dusk surveys coincided with spring low tide such that flooding of intertidal areas occurred between surveys. Thus, export of a benthic respiratory signal to surface waters would explain the net heterotrophy observed during both day and night intervals. This benthic respiratory signal could result from several processes including 1) direct entrainment into the shallow (~2 m) lens of surface water as it floods and ebbs over intertidal areas, 2) export from shallow subtidal sediments to subpycnal waters followed by mixing with surface waters at the fjord head or 3) exchange with Pillan Fjord. Supporting the latter process, Mulsow et al. (2006) reported intense remineralization of OC in surface sediments in Pillan Fjord due to the deposition of labile material from fish farms. Lower remineralization rates might be expected in intertidal areas of the delta, which has been formed primarily from inorganic sediment. Yet, significant benthic respiration could still occur if organic matter from nearby fish farms or riverine sources is deposited in shallow sediments. Silva et al. (2011) found that deep sediments in upper Reñihue had the lowest OC content in the northeastern CIS but also had a similar proportion of terrestrial material to Reloncaví Fjord. The lower OC content may be linked to additional degradation of organic matter in shallow waters prior to longer term storage in deeper waters, albeit one of many potential explanations. Silva et al. (2011) also found that sediments in lower Reñihue (near station N4) had the highest OC content and most marine origin among the three fjords. While the authors' results from sediment samples represent much longer timescales, they are nevertheless consistent with the finer resolution results from this study that show the lower Reñihue is the most productive, marine-dominated fjord among the three study systems.

4.4. Implications of climate change for carbon storage and aquaculture in Patagonian fjords

The poleward shift of westerly winds since the 1970s is predicted to continue through at least mid-century with the northern Patagonia fjord system experiencing the strongest impacts (Garreaud et al., 2013). The two primary effects on geophysical drivers in fjords include a reduction in river discharge of 5–20% primarily occurring in summer-autumn (Aguayo et al., 2019; Aguayo et al., 2021) and increasing dominance of synoptic wind forcing due to weaker zonal winds (Garreaud et al., 2013; Pérez-Santos et al., 2019). Environmental forcing during the study period exemplifies these conditions, e.g., synoptic winds were dominant and the 2018 Puelo River discharge during late summer-autumn 2018 was ~10% lower than the decadal mean. Accordingly, the key functional relationships observed in this study provide insight on how Patagonian fjords will respond to future trends.

4.4.1. Transfer of planktonic carbon to coastal sediments shifts landward from CIS into fjords

The impact of reduced discharge from the Puelo River is the most pronounced given its extensive influence throughout the northern CIS. Weaker stratification and stronger synoptic forcing in upper Reloncaví Fjord increase upwelling and primary production (Section 4.1). This autochthonous OC is more likely to be retained in the fjord compared to under high discharge conditions which suppress upwelling, limit light and nutrient availability and quickly export surface OC production to the CIS. Lower freshwater input to Comau Fjord is less likely to drive a significant metabolic shift, especially when the nutricline is well below the pycnocline, as observed in this study. However, it is logical that import of planktonic OC from the Ancud Gulf would increase under stronger synoptic forcing (Section 4.2). The relatively low energy conditions in Comau between synoptic cycles may then act as an efficient trap by which detrital OC is transferred to sediments. Supporting this mechanism, Mayr et al. (2014) and Rebolledo et al. (2015) found that accumulation of planktonic OC in sediments from Comau and upper Reloncaví Fjords has increased in recent decades corresponding to decreased river discharge. Over the same period, marine OC accumulation in the eastern Gulf of Ancud has decreased (Rebolledo et al., 2011). Thus, both sediment and geophysical process studies imply a mechanism by which deposition of planktonic OC shifts landward from the eastern CIS and into fjords. Whether this shift translates to higher OC retention overall, e.g., due to greater depths in fjords, remains a question for further sediment and carbon budget studies.

4.4.2. Greater biogeochemical variability presents management challenges for aquaculture

High river discharge and strong zonal winds establish a well-stratified water column that can be beneficial for aquaculture, e.g., reducing potential for harmful algal blooms (León-Muñoz et al., 2018) or providing a stable layer with optimal aragonite saturation for shellfish aquaculture (Vergara-Jara et al., 2019; Yevenes et al., 2019). Lower river discharge and stronger synoptic forcing due to climate change will enhance local upwelling/downwelling in fjords and decrease flushing times. While it is possible that these changes may have some benefits, they may also present greater risks and variability that will be more challenging to manage. For example, upwelling in Reloncaví Fjord can increase planktonic food sources, but it also increases the potential for harmful algal blooms and exposes shellfish to low aragonite saturation that is suboptimal for growth (León-Muñoz et al., 2018; Yevenes et al., 2019). Additionally, it is more difficult to predict and adaptively manage for upwelling events that vary with synoptic forcing over weekly scales rather than seasonal forcing from zonal winds. In Comau Fjord, lower freshwater input and stronger up-fjord winds may further increase flushing times and persistence of nutrient-deplete conditions. As a result, input of nutrients or pathogens from aquaculture may have a more localized and direct impact (Iriarte et al., 2013; Olsen et al., 2014, Olsen et al., 2017; Soto et al., 2021). On the other hand, tidally dominated systems like Reñihue Fjord are less likely to be impacted by altered river flow and synoptic winds, as conditions are more closely linked to regional ocean processes. The contrasting response among the three fjords to predicted climatic change underscores the need for knowledge and tools to assess site-specific vulnerability for aquaculture adaptation and management.

4.5. Conclusions

This study examined how diverse geophysical characteristics and environmental forcing were coupled to metabolic processes in the three northernmost Patagonian fjords and how this biogeochemical functioning varied within and between these fjords. Synthesis of high-resolution observations, monitoring data, models and historical data

support the following conclusions:

- *The dominant control (river input, winds, tides) on surface waters < 30 m differed in each of the three northernmost fjords in Patagonia, reflecting the fundamental influence of geomorphologic setting as a master variable on ecosystem function.* Biogeochemical cycling was further mediated by characteristics along the river-fjord continuum, such as the presence of hydrologic reservoirs and head deltas.

- *Similar forcing conditions can lead to contrasting physical-metabolic responses between fjords, particularly depending on fjord orientation and location of riverine input.* For example, northerly winds enhanced upwelling and net autotrophy in upper Reloncaví Fjord but deepened the nutrient-deplete surface layer in Comau Fjord thereby sustaining nutrient limitation in the euphotic zone.

- *Metabolic balance within individual fjords is strongly influenced by connectivity to other fjords, gulfs and channels within the CIS.* Salt fingering in Comau Fjord and its potential role as a major nutrient source to the euphotic zone were linked to physical processes and nutrient depletion in the Gulf of Ancud over synoptic to seasonal scales. High metabolic rates in lower Reñihue were linked to vertical mixing of nutrient-rich waters to the surface in the Desertores Islands over tidal scales.

- *Decreased river discharge due to climate change will enhance the relative role of wind forcing on fjord surface waters, driving higher biogeochemical variability over synoptic scales and shifting depositional pathways for autochthonous OC.* This change will be most pronounced in river-dominated fjords like Reloncaví, and least significant in tide-dominated fjords like Reñihue.

The unique geophysical-metabolic coupling among the three fjords in the northern CIS highlights the challenge of resolving these processes at relevant scales for the management of local and globally-significant ecosystem services. Addressing this challenge will require regional models that constrain function and connectivity at seasonal scales but also support downscaling to fine-scale forcing in fjords. Development of these modelling and management tools will depend on integrated observational efforts that continue to refine our mechanistic understanding of fjord function through process studies, remote sensing and long-term monitoring.

CRediT authorship contribution statement

Joseph R. Crosswell: Conceptualization, Supervision, Writing – original draft, Writing – review & editing. **Francisco Bravo:** Resources, Writing – review & editing. **Iván Pérez-Santos:** Writing – review & editing. **Geoffrey Carlin:** Methodology. **Nagur Cherukuru:** Writing – review & editing. **Cassie Schwanger:** . **Rob Gregor:** . **Andrew D.L. Steven:** Conceptualization, Writing – review & editing, Funding acquisition.

Declaration of Competing Interest

The authors declare that they have no known competing financial interests or personal relationships that could have appeared to influence the work reported in this paper.

Data availability

Data presented in this manuscript are a subset of data collected during the SIMA_2018_V01 voyage (Crosswell, 2018). This voyage dataset is available via CSIRO's Data Access Portal (https://doi.org/10.25919/60tt-x362).

Acknowledgements

This work was supported by funding from the Ministry of Economy of Chile and Fondo de Inversión Estratégica FIE as part of the SIMA Austral project. We greatly appreciate SERNAPESCA, IFOP and Stacy Ballyram/Huinay Research Station for support throughout the fieldwork campaigns, including use of laboratory facilities, logistical assistance, data access and scientific insight. We thank Diego Ocampo at CSIRO Chile for support with logistics, sampling and data management, and we thank Kate Hodge at Hodge Environmental for illustration of conceptual diagrams. We are grateful for helpful discussions with Oscar Sepúlveda-Steiner as well as with Mike Herzfeld, Farhan Rizwi and the entire CSIRO Coastal Environmental Modelling group and Coastal Informatics team. Finally, this work would not have been possible without the support of Fernando Ogalde and the crew of R/V Khronos.

Appendix A. Supplementary data

Supplementary data to this article can be found online at https://doi.org/10.1016/j.pocean.2022.102866.

References

Aguayo, R., León-Muñoz, J., Vargas-Baecheler, J., Montecinos, A., Garreaud, R., Urbina, M., Iriarte, J.L., 2019. The glass half-empty: climate change drives lower freshwater input in the coastal system of the Chilean Northern Patagonia. Climatic Change 155 (3), 417–435. https://doi.org/10.1007/s10584-019-02495-6.

Aguayo, R., León-Muñoz, J., Garreaud, R., Montecinos, A., 2021. Hydrological droughts in the southern Andes (40–45° S) from an ensemble experiment using CMIP5 and CMIP6 models. Scientific reports 11 (1), 1–16. https://doi.org/10.1038/s41598-021-84807-4.

Aiken, C.M., 2012. Seasonal thermal structure and exchange in Baker Channel, Chile. Dynamics of Atmospheres and Oceans 58, 1–19.

Almonacid PM, Medel C (2020) A structure-preserving numerical approach for simulating algae blooms in marine water bodies of western Patagonia. arXiv preprint arXiv:2007.11815.

Aracena, C., Lange, C., Iriarte, J.L., Rebolledo, L., Pantoja, S., 2011. Latitudinal patterns of export production recorded in surface sediments of the Chilean Patagonian fjords (41–551S) as a response to water column productivity. Continental Shelf Research 31, 340–355. https://doi.org/10.1016/j.csr.2010.08.008.

Arneborg, L., Liljebladh, B., 2001. The internal seiches in Gullmar Fjord. Part II: Contribution to basin water mixing. Journal of Physical Oceanography 31, 2567–2574.

Baines, P.G., 1982. On internal tide generation models. Deep Sea Research Part A, Oceanographic Research Papers 29, 307–338.

Banko-Kubis, H.M., Wurl, O., Mustaffa, N.I.H., Ribas-Ribas, M., 2019. Gas transfer velocities in Norwegian fjords and the adjacent North Atlantic waters. Oceanologia 61, 460–470.

Behrenfeld, M.J., Falkowski, P.G., 1997. Photosynthetic rates derived from satellite-based chlorophyll concentration. Limnology and oceanography 42, 1–20.

Behrenfeld, M.J., Marañón, E., Siegel, D.A., Hooker, S.B., 2002. Photoacclimation and nutrient-based model of light-saturated photosynthesis for quantifying oceanic primary production. Marine Ecology Progress Series 228, 103–117.

Bianchi, T.S., Arndt, S., Austin, W.E.N., Benn, D.I., Bertrand, S., Cui, X., Faust, J.C., Koziorowska-Makuch, K., Moy, C.M., Savage, C., Smeaton, C., Smith, R.W., Syvitski, J., 2020. Fjords as Aquatic Critical Zones (ACZs). Earth-Science Reviews 203, 103145.

Calvete, C., Sobarzo, M., 2011. Quantification of the surface brackish water layer and frontal zones in southern Chilean fjords between Boca del Guafo (43°30'S) and Estero Elefantes (46°30'S). Cont Shelf Res 31, 162–171. https://doi.org/10.1016/j.csr.2010.09.013.

Castillo, M.I., Pizarro, O., Cifuentes, U., Ramirez, N., Djurfeldt, L., 2012. Subtidal dynamics in a deep fjord of southern Chile. Cont Shelf Res 49, 73–89.

Castillo, M.I., Cifuentes, U., Pizarro, O., Djurfeldt, L., Caceres, M., 2016. Seasonal hydrography and surface outflow in a fjord with a deep sill: The Reloncaví fjord, Chile. Ocean Science 12, 533–534.

Castillo, M.I., Pizarro, O., Ramírez, N., Cáceres, M., 2017. Seiche excitation in a highly stratified fjord of southern Chile: The Reloncaví fjord. Ocean Science 13, 145–160.

Clementson L, Malthus T, Cherukuru N, Crosswell J, Steven A, Bernal P, Ocampo D, Wojtasiewicz B, Brewer E (2020): Bio-optical Data from Chilean Coastal waters 2017 - 2020. v1. CSIRO. Data Collection. https://doi.org/10.25919/qbbv-v359.

Cloern, J.E., Foster, S.Q., Kleckner, A.E., 2014. Phytoplankton primary production in the world's estuarine-coastal ecosystems. Biogeosciences 11 (9), 2477–2501.

Collins, A.K., Allen, S.E., Pawlowicz, R., 2009. The role of wind in determining the timing of the spring bloom in the Strait of Georgia. Canadian Journal of Fisheries and Aquatic Sciences 66, 1597–1616.

Cottier, F.R., Nilsen, F., Skogseth, R., Tverberg, V., Skardhamar, J., Svendsen, H., 2010. Arctic fjords: A review of the oceanographic environment and dominant physical processes. Geological Society Special Publication 344, 35–50.

Crawford, D.W., Montero, P., Daneri, G., 2021. Blooms of Alexandrium catenella in Coastal Waters of Chilean Patagonia: Is Subantarctic Surface Water Involved? Frontiers in Marine Science 8, 326.
Crosswell, J.R., Anderson, I.C., Stanhope, J.W., Van, D.B., Brush, M.J., Ensign, S., Piehler, M.F., McKee, B., Bost, M., Paerl, H.W., 2017. Carbon budget of a shallow, lagoonal estuary: Transformations and source-sink dynamics along the river-estuary-ocean continuum. Limnology and Oceanography 62, S29–S45. https://doi.org/10.1002/lno.10631.
Crosswell, J.R., Carlin, G., Steven, A., 2020. Controls on carbon, nutrient, and sediment cycling in a large, semiarid estuarine system; princess Charlotte Bay. Australia. Journal of Geophysical Research: Biogeosciences 125:e2019JG005049. https://doi.org/10.1029/2019JG005049.
Crosswell J (2017) Sampling summary for SIMA validation voyage Oct 2017. CSIRO: CSIRO; 2017. https://doi.org/10.25919/zrr5-t267.
Crosswell, J (2018) Sampling summary for SIMA validation voyage, March-April 2018. CSIRO: CSIRO; 2018. https://doi.org/10.25919/2gst-je40.
Cushman-Roisin, B., Asplin, L., Svendsen, H., 1994. Upwelling in broad fjords. Cont Shelf Res 14.
Daneri, G., Montero, P., Lizárraga, L., Torres, R., Iriarte, J., Jacob, B., González, H., Tapia, F., 2012. Primary productivity and heterotrophic activity in an enclosed marine area of central Patagonia (Puyuhuapi channel; 44 S, 73 W). Biogeosciences Discussions 9, 5929–5968.
Dávila, P.M., Figueroa, D., Müller, E., 2002. Freshwater input into the coastal ocean and its relation with the salinity distribution off austral Chile (35–55 S). Cont Shelf Res 22, 521–534.
Dokulil, M.T., Qian, K., 2021. Photosynthesis, carbon acquisition and primary productivity of phytoplankton: a review dedicated to Colin Reynolds. Hydrobiologia 848, 77–94.
FAO (2020) The State of World Fisheries and Aquaculture 2020. Sustainability in action. Rome. https://doi.org/10.4060/ca9229en.
Farmer, D.M., Freeland, H.J., 1983. The physical oceanography of Fjords. Progress in Oceanography 12, 147–220.
Fillinger, L., Richter, C., 2013. Vertical and horizontal distribution of desmophyllum dianthus in Comau Fjord, Chile: A cold-water coral thriving at low pH. PeerJ 2013, 1–22.
Garreaud, R., Lopez, P., Minvielle, M., Rojas, M., 2013. Large-scale control on the Patagonian climate. Journal of Climate 26 (1), 215–230. https://doi.org/10.1175/JCLI-D-12-00001.1.
Geyer, W.R., Ralston, D.K., 2011. The dynamics of strongly stratified estuaries. Elsevier, Treatise on Estuarine and Coastal Science. Amsterdam, pp. 37–52.
Goebel, N.L., Wing, S.R., Boyd, P.W., 2005. A mechanism for onset of diatom blooms in a fjord with persistent salinity stratification. Estuar Coast Shelf Sci 64, 546–560.
González, H., Calderón, M., Castro, L., Clement, A., Cuevas, L., Daneri, G., Iriarte, J., Lizárraga, L., Martínez, R., Menschel, E., et al., 2010. Primary production and plankton dynamics in the Reloncaví Fjord and the Interior Sea of Chiloé, Northern Patagonia, Chile. Marine Ecology Progress Series 402, 13–30.
González, H., Castro, L., Daneri, G., Iriarte, J., Silva, N., Vargas, C., Giesecke, R., Sánchez, N., 2011. Seasonal plankton variability in Chilean Patagonia fjords: carbon flow through the pelagic food web of Aysen Fjord and plankton dynamics in the Moraleda Channel basin. Cont Shelf Res 31, 225–243.
González, H., Castro, L., Daneri, G., Iriarte, J., Silva, N., Tapia, F., Teca, E., Vargas, C., 2013. Land-ocean gradient in haline stratification and its effects on plankton dynamics and trophic carbon fluxes in Chilean Patagonian fjords (47–50 S). Progress in oceanography 119, 32–47.
González, H., Graeve, M., Kattner, G., Silva, N., Castro, L., Iriarte, J., Osmán, L., Daneri, G., Vargas, C., 2016. Carbon flow through the pelagic food web in southern Chilean Patagonia: relevance of Euphausia vallentini as a key species. Marine Ecology Progress Series 557, 91–110.
González, H.E., Nimptsch, J., Giesecke, R., Silva, N., 2019. Organic matter distribution, composition and its possible fate in the Chilean North-Patagonian estuarine system. Science of the Total Environment 657, 1419–1431.
Gorton, R., Condie, S., 2018. SIMA Austral Dispersal and Connectivity Modelling in the Los Lagos Region. In: Steven, A.D.L. (Ed.), SIMA-Austral FIE V008- Integrated Ecosystem-based Sanitary and Environmental Management System for Aquaculture. CSIRO, Final Report, p. 178.
Herzfeld, M., 2006. An alternative coordinate system for solving finite difference ocean models. Ocean Modelling 14, 174–196.
Herzfeld, M., 2018. SIMA Austral Hydrodynamic Model Technical Report. In: Steven, A. D.L. (Ed.), SIMA-Austral FIE V008- Integrated Ecosystem-based Sanitary and Environmental Management System for Aquaculture. CSIRO, Final Report, p. 178.
Hopwood, M.J., Carroll, D., Dunse, T., Hodson, A., Holding, J.M., Iriarte, J.L., Meire, L., 2020. How does glacier discharge affect marine biogeochemistry and primary production in the Arctic? The Cryosphere 14 (4), 1347–1383.
Hughes, D.J., Campbell, D.A., Doblin, M.A., Kromkamp, J.C., Lawrenz, E., Moore, C.M., Oxborough, K., Prášil, O., Ralph, P.J., Alvarez, M.F., Suggett, D.J., 2018. Roadmaps and Detours: Active Chlorophyll- a Assessments of Primary Productivity Across Marine and Freshwater Systems. Environmental Science and Technology 52, 12039–12054.
Inall, M., Gillibrand, P., 2010. The physics of mid-latitude fjords: a review. Geological Society, London, Special Publications 344, 17–33.
IOC et al. (2010) IOC, SCOR and IAPSO: The International Thermodynamic Equation of Seawater – 2010: Calculation and Use of Thermodynamic Properties. Intergovernmental Oceanographic Commission, Manuals and Guides No. 56, UNESCO (English), 196 pp.
Iriarte, J.L., 2018. Natural and human influences on marine processes in Patagonian subantarctic coastal waters. Frontiers in Marine Science 5, 1–7.
Iriarte J, González H (2008) Phytoplankton bloom ecology of the inner Sea of Chiloé, Southern Chile. Nova Hedwigia:67–79.
Iriarte JL, Cuevas LA, Cornejo F, Silva N, González HE, Castro L, Montero P, Vargas CA, Daneri G (2018) Low spring primary production and microplankton carbon biomass in Sub-Antarctic Patagonian channels and fjords (50–53°S). Arctic, Antarctic, and Alpine Research 50.
Iriarte, J.L., Gonzlez, H.E., Nahuelhual, L., 2010. Patagonian fjord ecosystems in Southern Chile as a highly vulnerable region: Problems and needs. Ambio 39, 463–466.
Iriarte, J.L., Pantoja, S., González, H.E., Silva, G., Paves, H., Labbé, P., Rebolledo, L., Van, A.M., Häussermann, V., 2013. Assessing the micro-phytoplankton response to nitrate in Comau Fjord (42 S) in Patagonia (Chile), using a microcosms approach. Environmental Monitoring and Assessment 185, 5055–5070.
Iriarte, J.L., Pantoja, S., Daneri, G., 2014. Oceanographic Processes in Chilean Fjords of Patagonia: From small to large-scale studies. Progress in Oceanography 129, 1–7. https://doi.org/10.1016/j.pocean.2014.10.004.
Iriarte, J.L., León-Muñoz, J., Marcé, R., Clément, A., Lara, C., 2017. Influence of seasonal freshwater streamflow regimes on phytoplankton blooms in a Patagonian fjord. New Zealand Journal of Marine and Freshwater Research 51, 304–315.
Jassby, A.D., Platt, T., 1976. Mathematical formulation of the relationship between photosynthesis and light for phytoplankton. Limnology and Oceanography 21, 540–547.
Laudien, J., Häussermann, V., Försterra, G., Goehlich, H., 2014. Physical oceanographic profiles of seven CTD casts from Gulf of Ancud into Comau Fjord in 2014. Alfred Wegener Institute, Helmholtz Centre for Polar and Marine Research, Bremerhaven, PANGAEA,. https://doi.org/10.1594/PANGAEA.832187.
Laudien, J., Jantzen, C., Häussermann, V., Försterra, G., Sswat, M., Baumgarten, S., Richter, C., 2017a. Physical oceanographic profiles of seven CTD casts from Gulf of Ancud into Comau Fjord in 2011. Alfred Wegener Institute, Helmholtz Centre for Polar and Marine Research, Bremerhaven, PANGAEA,. https://doi.org/10.1594/PANGAEA.884120.
Laudien, J., Häussermann, V., Försterra, G., Goehlich, H., 2017b. Physical oceanographic profiles of 14 CTD casts from Gulf of Ancud into Comau Fjord in 2013. Alfred Wegener Institute, Helmholtz Centre for Polar and Marine Research, Bremerhaven, PANGAEA,. https://doi.org/10.1594/PANGAEA.874259.
Laudien, J., González-Diaz, F., Goehlich, H., 2017c. Physical oceanographic profiles of six CTD casts from Reñihue Fjord in 2013. Alfred Wegener Institute, Helmholtz Centre for Polar and Marine Research, Bremerhaven, PANGAEA,. https://doi.org/10.1594/PANGAEA.874261.
Lehrter, J.C., Cebrian, J., 2010. Uncertainty propagation in an ecosystem nutrient budget. Ecological Applications 20 (2), 508–524.
León-Muñoz, J., Marcé, R., Iriarte, J., 2013. Influence of hydrological regime of an Andean river on salinity, temperature and oxygen in a Patagonia fjord, Chile. New Zealand Journal of Marine and Freshwater Research 47, 515–528.
León-Muñoz, J., Urbina, M.A., Garreaud, R., Iriarte, J.L., 2018. Hydroclimatic conditions trigger record harmful algal bloom in western Patagonia (summer 2016). Scientific reports 8 (1), 1–10. https://doi.org/10.1038/s41598-018-19461-4.
Lindahl, O., Belgrano, A., Davidsson, L., Hernroth, B., 1998. Primary production, climatic oscillations, and physico-chemical processes: The Gullmar Fjord time-series data set (1985–1996). ICES Journal of Marine Science 55, 723–729.
Marshall, M.G., Kellerman, A.M., Wadham, J.L., Hawkings, J.R., Daneri, G., Torres, R., Spencer, R.G., 2021. Seasonal changes in dissolved organic matter composition in a Patagonian fjord affected by glacier melt inputs. Frontiers in Marine Science 8, 612386.
Mayr, C.C., Försterra, G., Häussermann, V., Wunderlich, A., Grau, J., Zieringer, M., Altenbach, A.V., 2011. Stable isotope variability in a Chilean fjord food web: implications for N-and C-cycles. Marine Ecology Progress Series 428, 89–104.
Mayr, C., Rebolledo, L., Schulte, K., Schuster, A., Zolitschka, B., Försterra, G., Häussermann, V., 2014. Responses of nitrogen and carbon deposition rates in Comau Fjord (42°S, southern Chile) to natural and anthropogenic impacts during the last century. Cont Shelf Res 78, 29–38.
McDougall, T.J., Barker, P.M., 2011. Getting started with TEOS-10 and the Gibbs Seawater (GSW) oceanographic toolbox. SCOR/IAPSO WG 127, 1–28.
Millero, F.J., 2010. Carbonate constants for estuarine waters. Marine and Freshwater Research 61, 139–142. https://doi.org/10.1071/mf09254.
Moffat, C., 2014. Wind-driven modulation of warm water supply to a proglacial fjord, Jorge Montt Glacier, Patagonia. Geophysical Research Letters 41, 3943–3950.
Montero, P., Daneri, G., González, H.E., Iriarte, J.L., Tapia, F.J., Lizárraga, L., Sanchez, N., Pizarro, O., 2011. Seasonal variability of primary production in a fjord ecosystem of the Chilean Patagonia: Implications for the transfer of carbon within pelagic food webs. Cont Shelf Res 31, 202–215.
Montero, P., Pérez-Santos, I., Daneri, G., Gutiérrez, M.H., Igor, G., Seguel, R., Purdie, D., Crawford, D.W., 2017. A winter dinoflagellate bloom drives high rates of primary production in a Patagonian fjord ecosystem. Estuar Coast Shelf Sci 199, 105–116.
Müller J (2012) The Two Mytilids Aulacomya atra and Mytilus chilensis from the Chilean Fjord Region: Aspects of Population Dynamics, Production and Metabolism. Doctoral dissertation, Christian-Albrechts-Universität zu Kiel.
Mulsow, S., Krieger, Y., Kennedy, R., 2006. Sediment profile imaging (SPI) and micro-electrode technologies in impact assessment studies: Example from two fjords in Southern Chile used for fish farming. Journal of Marine Systems 62, 152–163.
Muñoz, P., Sellanes, J., Villalobos, K., Zapata-Hernández, G., Mayr, C., Araya, K., 2014. Geochemistry of reduced fluids from shallow cold vents hosting chemosynthetic communities (Comau Fjord, Chilean Patagonia,~ 42° S). Progress in Oceanography, 129,:159–169.
Narváez, D.A., Vargas, C.A., Cuevas, L.A., García-Loyola, S.A., Lara, C., Segura, C., Tapia, F.J., Broitman, B.R., 2019. Dominant scales of subtidal variability in coastal

hydrography of the Northern Chilean Patagonia. Journal of Marine Systems 193, 59–73.
Olsen, L.M., Hernández, K.L., van Ardelan, M., Iriarte, J.L., Sánchez, N., González, H.E., Tokle, N., Olsen, Y., 2014. Responses in the microbial food web to increased rates of nutrient supply in a southern Chilean fjord: Possible implications of cage aquaculture. Aquaculture Environment Interactions 6, 11–27.
Olsen, L.M., Hernández, K.L., Ardelan, M.V., Iriarte, J.L., Bizsel, K.C., Olsen, Y., 2017. Responses in bacterial community structure to waste nutrients from aquaculture: An in situ microcosm experiment in a Chilean fjord. Aquaculture Environment Interactions 9, 21–32.
Pérez-Santos, I., Garcés-Vargas, J., Schneider, W., Ross, L., Parra, S., Valle-Levinson, A., 2014. Double-diffusive layering and mixing in Patagonian fjords. Progress in Oceanography 129, 35–49.
Pérez-Santos, I., Seguel, R., Schneider, W., Linford, P., Donoso, D., Navarro, E., Amaya-Cárcamo, C., Pinilla, E., Daneri, G., 2019. Synoptic-scale variability of surface winds and ocean response to atmospheric forcing in the eastern austral pacific ocean. Ocean Science 15, 1247–1266.
Pérez-Santos, I., Díaz, P.A., Silva, N., Garreaud, R., Montero, P., Henríquez-Castillo, C., Barrera, F., Linford, P., Amaya, C., Contreras, S., Aracena, C., Pinilla, E., Altamirano, R., Vallejos, L., Pavez, J., Maulen, J., 2021. Oceanography time series reveals annual asynchrony input between oceanic and estuarine waters in Patagonian fjords. Science of the Total Environment 798, 149241.
Pinilla, E., Castillo, M.I., Pérez-Santos, I., Venegas, O., Valle-Levinson, A., 2020. Water age variability in a Patagonian fjord. Journal of Marine Systems 210, 103376.
Quiroga E, Ortiz P, González-Sald'\ias R, Reid B, Tapia FJ, Pérez-Santos I, Rebolledo L, Mansilla R, Pineda C, Cari I, others (2016) Seasonal benthic patterns in a glacial Patagonian fjord: the role of suspended sediment and terrestrial organic matter. Marine Ecology Progress Series 561:31–50.
Rebolledo, L., González, H.E., Muñoz, P., Iriarte, J.L., Lange, C., Pantoja, S., Salamanca, M., 2011. Siliceous productivity changes in Gulf of Ancud sediments (42° S, 72° W), southern Chile, over the last ~150 years. Cont. Shelf Res. 31, 356–365. https://doi.org/10.1016/j.csr.2010.06.015.
Rebolledo, L., Lange, C.B., Bertrand, S., Muñoz, P., Salamanca, M., Lazo, P., Dezileau, L., 2015. Late Holocene precipitation variability recorded in the sediments of Reloncaví Fjord (41 S, 72 W). Chile. Quaternary Research 84 (1), 21–36. https://doi.org/10.1016/j.yqres.2015.05.006.
Reche, P., Artal, O., Pinilla, E., Ruiz, C., Venegas, O., Arriagada, A., Falvey, M., 2021. CHONOS: Oceanographic information website for Chilean Patagonia. Ocean & Coastal Management 208, 105634. https://doi.org/10.1016/j.ocecoaman.2021.105634.
Regaudie-de-Gioux, A., Lasternas, S., Agustí, S., Duarte, C.M., 2014. Comparing marine primary production estimates through different methods and development of conversion equations. Frontiers in Marine Science 1, 1–14.
Ruiz, C., Artal, O., Pinilla, E., Sepúlveda, H.H., 2021. Stratification and mixing in the Chilean Inland Sea using an operational model. Ocean Modelling 158, 101750.
Saggiomo, V., Santarpia, I., Saggiomo, M., Margiotta, F., Mangoni, O., 2011. Primary production processes and photosynthetic performance of a unique periantarctic ecosystem: The Strait of Magellan. Polar Biology 34, 1255–1267.
Saldías, G.S., Hernández, W., Lara, C., Muñoz, R., Rojas, C., Vásquez, S., Pérez-Santos, I., Soto-Mardones, L., 2021. Seasonal variability of sst fronts in the inner sea of chiloé and its adjacent coastal ocean, Northern Patagonia. Remote Sensing 13, 1–12.
Schneider, W., Pérez-Santos, I., Ross, L., Bravo, L., Seguel, R., Hernández, F., 2014. On the hydrography of Puyuhuapi Channel, Chilean Patagonia. Progress in Oceanography 129, 8–18. https://doi.org/10.1016/j.pocean.2014.03.007.
Seifert, M., Hoppema, M., Burau, C., Elmer, C., Friedrichs, A., Geuer, J.K., Iversen, M.H., 2019. Influence of glacial meltwater on summer biogeochemical cycles in Scoresby Sund. East Greenland. Frontiers in Marine Science 6, 412.
Sepúlveda, J., Pantoja, S., Hughen, K.A., 2011. Sources and distribution of organic matter in northern Patagonia fjords, Chile (~ 44–47 S): a multi-tracer approach for carbon cycling assessment. Continental Shelf Research 31 (3–4), 315–329. https://doi.org/10.1016/j.csr.2010.05.013.
Sepúlveda-Steiner, O., de La Fuente, A., Meruane, C., Bouffard, D., Wüest, A., 2015. Wind-driven baroclinic circulation effects over vertical mixing in a stratified Patagonian fjord. In Doctoral Dissertaion: Sepúlveda-Steiner. University of Chile.
Sievers, H.A., Silva, N., 2008. Water masses and circulation in austral Chilean channels and fjords. Progress in the Oceanographic Knowledge of Chilean Interior Waters. from Puerto Montt to Cape Horn. Comité Oceanográfico Nacional-Pontificia Universidad Católica de Valparaíso, Valparaíso:53–58.
Sievers H (2008) Temperature and Salinity in the Austral Chilean Channels and Fjords. Progress in the Oceanographic Knowledge of Chilean Interior Waters, from Puerto Montt to Cape Horn. Comité Oceanográfico Nacional-Pontificia Universidad Católica de Valparaíso, Valparaíso:31–36.
Silva, N., 2008. 3.2 dissolved oxygen, ph, and nutrients in the austral chilean channels and fjords. Progress in the oceanographic knowledge of Chilean interior waters. from Puerto Montt to Cape Horn. Comité Oceanográfico Nacional-Pontificia Universidad Católica de Valparaíso, Valparaíso:37.
Silva, N., Vargas, C.A., Prego, R., 2011. Land-ocean distribution of allochthonous organic matter in surface sediments of the Chiloé and Aysén interior seas (Chilean Northern Patagonia). Cont Shelf Res 31, 330–339.
Silva N (2008b) Physical and chemical characteristics of the surface sediments in the austral Chilean channels and fjords. Silva, N, Palma, S (Eds), Progress in the oceanographic knowledge of Chilean interior waters, from Puerto Montt to Cape Horn. Comité Oceanográfico Nacional-Pontificia Universidad Católica de Valparaíso, Valparaíso:69–75.
Skogseth, R., Sandvik, A.D., Asplin, L., 2007. Wind and tidal forcing on the meso-scale circulation in Storfjorden, Svalbard. Cont Shelf Res 27, 208–227.
Smith, R.W., Bianchi, T.S., Allison, M., Savage, C., Galy, V., 2015. High rates of organic carbon burial in fjord sediments globally. Nature Geoscience 8, 450–453.
Soto, D., León-Muñoz, J., Garreaud, R., Quiñones, R.A., Morey, F., 2021. Scientific warnings could help to reduce farmed salmon mortality due to harmful algal blooms. Marine Policy 132, 104705. https://doi.org/10.1016/j.marpol.2021.104705.
Spear, D.J., Thomson, R.E., 2012. Thermohaline staircases in a British Columbia fjord. Atmosphere - Ocean 50, 127–133.
Steven, A.D., Aryal, S., Bernal, P., Bravo, F., Bustamante, R.H., Condie, S., Dambacher, J. M., Dowideit, S., Fulton, E.A., Gorton, R., et al., 2019. SIMA Austral: An operational information system for managing the Chilean aquaculture industry with international application. Journal of Operational Oceanography:1–18.
Stigebrandt, A., 2012. In: Hydrodynamics and circulation of fjords. in Encyclopedia of Lakes and Reservoirs. Springer Science and Business Media B.V:, pp. 327–344. https://doi.org/10.1007/978-1-4020-4410-6.
Torres, R., Pantoja, S., Harada, N., González, H.E., Daneri, G., Frangopulos, M., Rutllant, J.A., Duarte, C.M., Rúiz-Halpern, S., Mayol, E., Fukasawa, M., 2011. Air-sea CO2 fluxes along the coast of Chile: From CO2 outgassing in central northern upwelling waters to CO2 uptake in southern Patagonian fjords. Journal of Geophysical Research: Oceans 116, 1–17.
Valle-Levinson, A., Sarkar, N., Sanay, R., Soto, D., León, J., 2007. Spatial structure of hydrography and flow in a Chilean fjord, Estuario Reloncaví. Estuaries and Coasts 30, 113–126.
Valle-Levinson, A., Caceres, M.A., Pizarro, O., 2014. Variations of tidally driven three-layer residual circulation in fjords. Ocean Dynamics 64, 459–469.
Vargas, C.A., Cuevas, L.A., Silva, N., González, H.E., De Pol-Holz, R., Narváez, D.A., 2018. Influence of glacier melting and river discharges on the nutrient distribution and DIC recycling in the Southern Chilean Patagonia. Journal of Geophysical Research: Biogeosciences 123, 256–270. https://doi.org/10.1002/2017JG003907.
Vásquez, S.I., de la Torre, M.B., Saldías, G.S., Montecinos, A., 2021. Meridional Changes in Satellite Chlorophyll and Fluorescence in Optically-Complex Coastal Waters of Northern Patagonia. Remote Sens. 13, 1026. https://doi.org/10.3390/rs13051026.
Vergara-Jara, M.J., DeGrandpre, M.D., Torres, R., Beatty, C.M., Cuevas, L.A., Alarcón, E., Iriarte, J.L., 2019. Seasonal Changes in Carbonate Saturation State and Air-Sea CO2 Fluxes During an Annual Cycle in a Stratified-Temperate Fjord (Reloncaví Fjord, Chilean Patagonia). Journal of Geophysical Research: Biogeosciences 124, 2851–2865.
Wanninkhof, R., 2014. Relationship between wind speed and gas exchange over the ocean revisited. Limnology and Oceanography: Methods 12, 351–362. https://doi.org/10.4319/lom.2014.12.351.
Weiss, R.F., 1974. Carbon dioxide in water and seawater: The solubility of a non-ideal gas. Marine Chemistry 2 (3), 203–215.
Yevenes, M.A., Lagos, N.A., Farías, L., Vargas, C.A., 2019. Greenhouse gases, nutrients and the carbonate system in the Reloncaví Fjord (Northern Chilean Patagonia): Implications on aquaculture of the mussel, Mytilus chilensis, during an episodic volcanic eruption. Science of the Total Environment 669, 49–61.